Hydrogen emissions from an electrolysis unit

by

Amanjot Kaur

Hydrogen emissions from an electrolysis unit

by

Amanjot Kaur

to obtain the degree of Master of Science in Sustainable Energy Technology
at the Delft University of Technology,
to be defended publicly on Thursday May 25, 2023 at 10:00 AM.

Student number:	5544092	
Project duration:	October 03, 2022 – May 25, 2023	
Thesis committee:	Prof. dr. ir. Ruud van Ommen,	TU Delft, Supervisor
	Ir. Ron Dobbelaar,	Worley, Supervisor
	Dr. Atul Bansode,	TU Delft

Abstract

Hydrogen is expected to play a vital role as an energy carrier in the future decarbonized system. Currently, a large portion of the hydrogen produced comes from the steam reforming of methane present in natural gas, which produces significant amounts of carbon dioxide emissions. However, with the growing need to reduce greenhouse gas emissions, a shift from fossil fuels to renewable energy sources is required. As a result, there is a growing emphasis on green hydrogen, i.e., hydrogen generated using renewable power. Green hydrogen has been growing at an exponential rate since 2020 and is expected to account for the majority of hydrogen production by 2050. However, a few studies have recently suggested that hydrogen may indirectly contribute to global warming. It is believed that hydrogen delays the decomposition of methane, a strong greenhouse gas, and thus extends its lifetime in the atmosphere. If green hydrogen is to be the primary fuel in the energy transition, hydrogen emissions from an electrolysis unit should be investigated.

This project focuses on identifying the sources of hydrogen emissions from an electrolysis unit. The goal is to comprehend the depth of this potential issue and investigate possible solutions. This project is carried out in collaboration with Worley, a market leader in the design, construction and delivery of green H_2 facilities. The leakage estimates for the green hydrogen alkaline electrolysis plant are based on Worley's in-house data. Venting during startup and shutdowns when power is unavailable, as well as hydrogen crossover in the electrolyzer, have been identified as two major contributors to hydrogen emissions. Solutions such as flaring systems to combust the vented hydrogen and battery energy systems to reduce frequent shutdowns and startups are investigated. To reduce emissions from hydrogen crossover, a reactor is modeled to explore the catalytic recombination of hydrogen and oxygen. These solutions are subjected to a techno-economic analysis to determine their viability.

Flare systems and battery energy systems are both deemed feasible. In the long run, however, installing a battery energy system would be preferable to combusting the hydrogen product. In comparison to other battery technologies such as Li-ion and lead-acid batteries, vanadium redox flow battery systems have been found to provide the maximum incentives and highest optimal capacities at the lowest overall costs. To avoid emissions from hydrogen crossover in a low-pressure alkaline electrolysis unit, the most cost-effective design involves a single-stage compression followed by a scrubber, heater, and reactor. However, this design is still costly because the annualized costs are four times greater than the costs offset by emissions reductions per year. Governments can encourage the adoption of such solutions by providing financial incentives to businesses.

Acknowledgements

I would like to express my gratitude to Ron Dobbelaar, my thesis supervisor at Company. This thesis would not be possible without his constant encouragement and support. He gave me enough time to figure things out on my own and helped me whenever I needed it. This thesis project, as well as working with him, has been an incredible journey that I have thoroughly enjoyed.

I'd also like to thank Prof. Ruud van Ommen, my thesis supervisor at TU Delft. He guided me every step of the way, from making the proposal to finishing the thesis. His adaptability and support have made the entire process so much smoother and less stressful.

I spent most of this time working at the company office in the Hague. I want to say a heartfelt thank you to everyone who has supported me at the company. They have patiently guided me and provided me with all the information I needed. They have inspired me at every turn of this journey, and I am very grateful for the opportunity to work with such wonderful colleagues.

I owe my friends both here and in India a debt of gratitude. They have been present during every stage. They have provided me with unwavering support throughout this journey, and I am sincerely grateful to have them by my side. I consider myself fortunate to be surrounded by such amazing people who always have my back.

Finally, I can't thank my mother, father, and brother enough. They have invested as much in this roller coaster ride as I have. They've laughed, cried, and rejoiced with me. I feel lucky to have such a supportive and loving family, and I want to dedicate this work to them. I would not have been able to achieve my goals without their love and encouragement. Their constant support has been my greatest source of strength throughout this journey.

Thank you all.

List of Symbols and Abbreviations

AACEI	Association for the Advancement of Cost Engineering International
AEM	Anion Exchange Membrane
AWE	Alkaline Water Electrolysis
BES	Battery Energy System
CAPEX	Capital Expenditure
CEPCI	Chemical Engineering Plant Cost Index
EPA	Environmental Protection Agency
EPC	Engineering Procurement & Construction
FGR	Flue Gas Recirculation
GHG	Greenhouse Gas
GW	Giga Watts
GWP	Global Warming Potential
HKN	Hollandse Kust Noord
IPCC	International Panel on Climate Change
LFP	Lithium Iron Phosphate
LHV	Lower Heating Value
MJ	Mega Joules
MW	Mega Watts
NCA	Nickel Cobalt Aluminium
NMC	Nickel Manganese Oxide
O&M	Operations & Maintenance
OPEX	Operational Expenditure
PDU	Purification and Drying Unit
PEM	Polymer Electrolyte Membrane
PPA	Power Purchase Agreement
PSV	Pressure Relief Valve
PV	Present Value
RD	Research & Development
SMR	Steam Methane Reforming
SoC	State of Charge
SOEC	Solid Oxide Electrolysis
TCI	Total Capital Investment
VRFB	Vanadium Flow Redox Batteries

ρ_f	Fluid density (kg/m^3)
C_{ref}	Capital recovery factor (-)
C	Bulk concentration of hydrogen (mol/m^3)
C_s	Concentration of hydrogen on catalyst surface (mol/m^3)
ϵ	Void fraction (-)
h_f	Heat transfer coefficient between fluid and catalyst particle (W/m^2·K)
Z	Annual interest rate (%)
t	Project lifetime (years)
d_p	Catalyst particle diameter (m)
a	External particle surface area per unit reactor volume (m^{-1})
f	Friction factor
ΔH_r	Heat of reaction (J/mol)
T_s	Catalyst temperature (K)
k_f	Mass transfer coefficient between fluid bulk and catalyst particle (m/s)
z	Reactor length coordinate (m)
R_v	Reaction rate per unit reactor volume (mol/m^3·s)
Re_p	Catalyst particle reynolds number
η	Catalyst effectiveness factor
R	Gas constant
μ	Viscosity (kg/m·s)
k	Rate constant (s^{-1})
Sh	Sherwood number
Sc	Schmidt number
P	System pressure (Pa)
T	Fluid temperature (K)
NOx	Nitrogen Oxides
u_s	Superficial gas velocity (m/s)
C_p	Heat capacity (J/mol·K)

List of Figures

List of Tables

Contents

1

Introduction

This chapter discusses the current situation as a result of climate change, as well as the need for green hydrogen to achieve the energy transition. The potential challenges posed by large-scale green hydrogen production are then discussed. Later, the motivation for this thesis project and its scope are discussed.

1.1. Climate change and green hydrogen

The Earth's temperature is rising at an alarming rate, resulting in rising sea levels, acidification of the oceans, melting glaciers, soil erosion, and other effects. According to the IPCC's (International Panel on Climate Change) sixth assessment report, the 10-year average temperature for the period 2013-2022 is estimated to be 1.14 °C above the 1800-1900 pre-industrial baseline. If the current trend continues, the global average temperature is expected to exceed 1.5°C within the next few decades. This climate change will result in severe environmental degradation, weather extremes, natural disasters, food insecurity, and numerous other disruptions. To slow down such extreme conditions, the temperature rise must be limited to 1.5°C. Limiting global warming to this temperature cannot be accomplished through business as usual; it would require significant technological and societal transformations in all sectors responsible for greenhouse gas emissions [1]. According to the IPCC, the energy sector accounts for two-thirds of greenhouse gas emissions, so there is an urgent need for a large-scale shift to renewable energy sources. All energy conversion, extraction, transmission, energy storage, and distribution processes comprises the energy sector. On December 12, 2015, 196 countries signed an agreement to achieve this energy transition at COP21 in Paris. The Paris Agreement aims to limit global warming to 1.5°C above pre-industrial levels. This is feasible if the world achieves carbon neutrality by the mid-century mark, i.e., zero net greenhouse gas emissions by 2050 [2].

The growing demand for decarbonization has fueled interest in green hydrogen, which is generated using renewable energy sources such as wind and solar power. Green hydrogen has the potential to significantly reduce carbon emissions and con-

tribute to meeting global climate goals. Green hydrogen must be deployed on a large scale to help decarbonize the energy sector. Globally, 120 million tonnes of hydrogen are produced annually, primarily for the methanol and ammonia industries. However, 95% of the hydrogen is produced from coal and natural gas, both of which emit significant amounts of carbon emissions. Only 5% of the hydrogen produced is obtained from the electrolysis of water, and only 1% of that is generated using renewable energy [3]. With continuous efforts from the public and private sectors, all currently used hydrogen is expected to be replaced by green hydrogen in existing applications. When combined with new applications as an alternative to conventional fuels in transportation, heating, and the steel production sector, green hydrogen will be dominant by 2050. The European hydrogen strategy aims to install 574 GW of electrolyzer capacity by 2050 in order to meet the Paris Agreement 2050. Global electrolyzer capacity is expected to reach 3075 GW by the mid-century mark [4].

1.2. Future Challenges

Hydrogen is expected to play a key role in decarbonizing our future energy system. However, there is growing evidence that hydrogen is an indirect greenhouse gas with a Global Warming Potential of 33 with respect to carbon dioxide. When hydrogen reaches the atmosphere, it reacts with the hydroxyl radicals (OH) present to form water. Certain Green House Gases (GHGs) such as methane are decomposed by these radicals in the atmosphere. H_2 molecules deplete the OH levels, delaying the decomposition of GHGs and lengthening their lifetime. Because H_2 molecules do not directly trap heat, they are referred to as indirect greenhouse gases. As a result, hydrogen leakage into the atmosphere may offset the benefits of a hydrogen-based future economy [1], [5].

1.3. Project Motivation and Scope

Hydrogen is difficult to contain, and a thorough understanding of the sources of leakage, as well as the amount of hydrogen that could be emitted into the atmosphere in a future energy system, is essential for a large-scale hydrogen economy. The hydrogen economy was not dominant in the conventional energy system, so this aspect of hydrogen is novel to the emerging renewable energy system and needs to be investigated, which motivates this project. The purpose of this thesis is to identify the major sources of hydrogen emissions in the electrolysis unit and to investigate potential technical solutions to reduce H_2 leakage. This project is carried out in collaboration with Worley, an EPC company active in green H_2 projects.

Green hydrogen can be produced using four electrolysis technologies: alkaline water electrolysis (AWE), polymer electrolyte membrane (PEM), anion exchange membrane (AEM), and solid oxide electrolysis (SOEC). Alkaline and PEM electrolysis technologies are commercially available. This project's estimates are all based on low-pressure alkaline electrolysis technology. First, a thorough literature review is conducted to identify potential leakage sources in production and comprehend

the impact of indirect global warming of hydrogen molecules. It is then followed by leakage calculations based on available data in the alkaline electrolysis unit. These estimates are compared to the carbon dioxide emissions from the grey hydrogen unit. Following that, a few solutions are proposed and modeled, and economic feasibility analysis is performed.

2

Green Hydrogen

This chapter provides an overview of water electrolysis as well as a brief discussion of leakage sources in the electrolysis unit. The discussion then shifts to the indirect global warming potential of hydrogen.

2.1. Electrolysis of Water

Electrolysis is the process of converting water into hydrogen and oxygen by using electricity. The hydrogen obtained using electricity from renewable sources of energy is termed "green hydrogen". The equipment in which electrolysis takes place is referred to as an "electrolyzer". It consists of two electrodes separated by an electrolyte, a medium for the transportation of anions or cations from one electrode to the other. The basic principle of water electrolysis is the same; however, differences in construction based on physio-chemical and electrochemical aspects result in four electrolyzer technologies. These are based on different electrolytes, membranes, operating temperatures, and pressures [6].

1) Alkaline water electrolysis(AWE): Since the early 1900s, it is the most applied technology. Alkaline electrolyzers have a lifespan of more than 15 years and are strong and dependable [7]. The most widely used electrolytes are sodium hydroxide (NaOH) and potassium hydroxide (KOH), which maintain the electrolyzer's pH at 14 [8]. Each electrolyzer cell consists of two electrodes, cathode and anode, which are separated from one another by a thin membrane called a diaphragm [9]. Water is reduced at the cathode to produce hydrogen and hydroxide ions. Hydroxide ions pass through the membrane towards the anode in the external electric field, where they recombine to produce oxygen. The following reactions take place in the alkaline electrolyzer [10]:

Cathode:

$$2\,H_2O(l) + 2\,e^- \longrightarrow H_2(g) + 2\,OH^-(aq) \tag{2.1}$$

Anode:

$$2\,OH^-(aq) \longrightarrow \frac{1}{2}\,O_2(g) + H_2O + 2\,e^- \tag{2.2}$$

The high-purity hydrogen (up to 99.99%) that can be obtained using this technology makes alkaline electrolyzers a popular choice for industrial-scale hydrogen production. The main advantage of using alkaline electrolysis is that it can be operated under ambient conditions due to which capital costs are low relative to other technologies like PEM and SOEC. The main drawbacks of this technology are the relatively low efficiency (around 70%), the corrosive nature of the highly alkaline electrolyte, and a long startup time [7], [11], [12]. Moreover, when operated with intermittent power and electrolyzers are shut down for an extended period of time (>48 hrs), units must be drained to prevent reverse polarization and attack on the electrode plating. The draining and filling of electrolyzers is a laborious and risky task. The alkaline electrolysis technology at the cell level is illustrated in Figure 2.1.

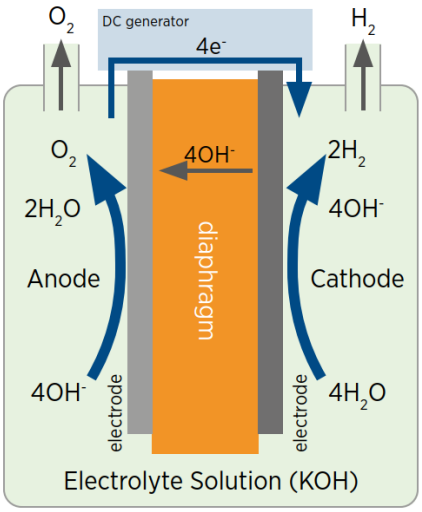

Figure 2.1: Alkaline electrolysis [6]

2) Polymer electrolyte membrane(PEM): After AWE, PEM electrolysis is the second most widely used for producing hydrogen. A solid polymer electrolyte is used in PEM electrolysis systems instead of corrosive chemicals. In addition, they are safer and more environmentally friendly than alkaline electrolysis because there is no alkaline fog in the hydrogen gas [7]. Protons are transferred from one electrode to another through a solid polymeric membrane. At the anode, water is oxidized to produce protons and oxygen. The membrane enables the transfer of protons from the anode to the cathode, and they combine to produce hydrogen gas at the cathode. The reactions occur as follows [10], [11]:

Cathode:

$$2\,H^+ + 2\,e^- \longrightarrow H_2(g) \tag{2.3}$$

Anode:

$$H_2O(l) \longrightarrow \frac{1}{2} O_2(g) + 2\,H^+(aq) + 2\,e^- \tag{2.4}$$

PEM electrolysis systems offer high-purity hydrogen and have higher efficiencies. They are better suited for the intermittent nature of renewable sources like solar and wind because of their fast response and short startup times. Additionally, PEM electrolysis systems are compact and modular, facilitating easy scalability and integration into the current infrastructure. These features make them a promising technology for the production of green hydrogen in the future. They have higher capital costs than alkaline electrolyzers as a result of the rare earth metals like Iridium used as catalysts in the electrodes [13]. The operating cost Figure 2.2 depicts the operation of a PEM electrolytic cell.

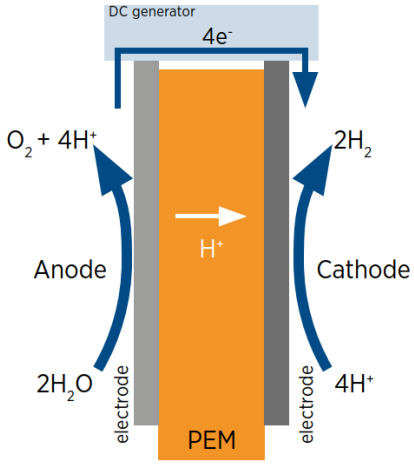

Figure 2.2: PEM electrolysis [6]

3) Anion exchange membrane(AEM): Anion exchange membrane electrolysis technology is still in the research phase currently, however, offers a promising future towards low-cost electrolysis. At the cathode, water is reduced to produce hydrogen gas and hydroxyl ions. The anion exchange membrane allows hydroxyl ions to diffuse to the anode side, where they recombine to form water and oxygen. The following half-cell reactions take place [14]:

Cathode:

$$4\,H_2O(l) + 4\,e^- \longrightarrow 2\,H_2(g) + 4\,OH^-(aq) \tag{2.5}$$

Anode:

$$4\,OH^-(aq) \longrightarrow O_2(g) + 2\,H_2O + 4\,e^- \tag{2.6}$$

The half-cell reactions occurring are identical to those in alkaline electrolysis, but the

main difference is the diffusion of hydroxyl ions. Alkaline electrolyzers use alkaline electrolytes for the transportation of hydroxyl ions, whereas polymer membranes are used in AEM for transporting anions [15]. AEM electrolysis may be more effective and economical than alkaline and PEM electrolysis because it operates at lower temperatures and uses more common materials in the electrodes. However, achieving high mechanical stability of AEM membranes along with high ionic conductivity is challenging and the main topic of research in order to scale up AEM electrolysis [16]. The functioning of an AEM electrolytic cell is shown in Figure 2.3.

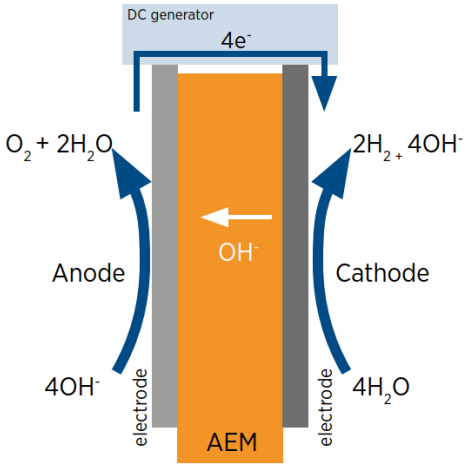

Figure 2.3: AEM electrolysis [6]

4) Solid oxide: Solid Oxide Electrolysis (SOEC) technology is under development currently. Compared to AWE and PEM electrolyzers, they are more efficient and have lower production costs for hydrogen gas. SOEC electrolyzers operate at high temperatures ranging from 500 to 1000 °C and the heat required can be supplied from sources like industrial waste heat [17]. They require less electrical energy in contrast to AWE and PEM electrolysis. Water is reduced to produce oxide anions and hydrogen gas at the cathode. Oxide anions flow through the solid ceramic electrolyte and recombine to form oxygen at the anode. The reactions require close contact of the electrodes with the vapor phase [7], [13].

Cathode:

$$H_2O(g) + 2\,e^- \longrightarrow H_2(g) + O_2^- \tag{2.7}$$

Anode:

$$O_2^- \longrightarrow \frac{1}{2}\,O_2(g) + 2\,e^- \tag{2.8}$$

Higher operating temperatures reduce kinetic and mass transfer limitations, allow-

ing for close to 100% efficiencies. SOEC has a few drawbacks, such as safety issues, and material degradation due to high temperatures. Despite these issues, solid-oxide technology offers a promising future in large-scale electrolysis and research is being done to enhance SOEC stability and develop durable materials that can be used in SOECs [18]. The solid oxide electrolytic cell is captured in Figure 2.4.

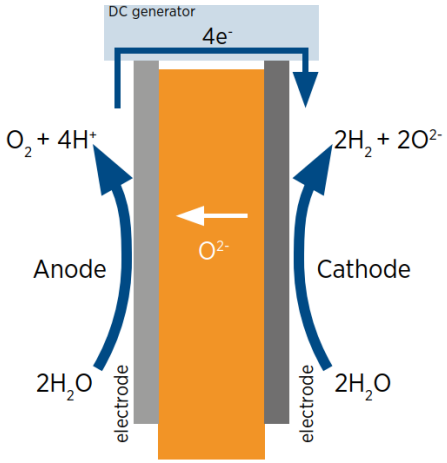

Figure 2.4: SOEC electrolysis [6]

Table 2.1 summarizes the key characteristics of all four types of electrolysis:

Table 2.1: Characteristics of different types of electrolysis [6], [10], [15]

	Unit	AWE	PEM	AEM	SOEC
Temperature range	°C	60-90	50-90	50-70	500-1000
Pressure range	bar	1-30	1-30	~30	<30
Efficiency	%	60-80	80	75	>90
H_2 purity	%	>99.8	99.99	99.99	99.99
Lifetime of system	year	20-30	10-20	-	-
Readiness	-	Mature	Commercial	R&D	Demonstration

2.2. Emission sources in the electrolysis unit

The future carbon-free economy is anticipated to rely heavily on green hydrogen. By 2050, it is expected that Europe will be able to produce 574 GW of hydrogen through water electrolysis. Due to its smaller size, hydrogen has the tendency to leak in large quantities during production. This section talks about the possible leakage sources in an electrolysis production unit. The following four main sources

of emissions that have been identified in the Frazer-Nash Consultancy report [1].

1) Venting at start-up and shutdown: Electrolyzers are designed to avoid the accumulation of a mixture of hydrogen and oxygen, which can be explosive. The lower explosive limit of hydrogen in an oxygen atmosphere is 4 wt% and hydrogen concentration is kept below 1% in order to maintain a sufficient safety margin. Any oxygen in the hydrogen side (cathode side) of the system must be removed during shutdowns to avoid the formation of an explosive gas mixture. The system is therefore vented and blanketed with nitrogen during shutdowns. The system is also vented during startup until all of the nitrogen has been removed. The amount of venting during startups and shutdowns can range from 0.0 to 0.6% of the total hydrogen produced annually[1].

2) Venting due to hydrogen cross-over: Hydrogen is generated at the cathode side of the electrolyzer system and oxygen at the anode side. Hydrogen is collected as a product, and currently, oxygen is mostly vented to the atmosphere. A small amount of hydrogen diffuses through the electrolyzer membrane from the cathode to the anode and ends up in the atmosphere along with oxygen. This is known as 'Hydrogen Cross-over". The main reason for this hydrogen crossover is the small size of the hydrogen molecule, and another reason could be if there is any pressure differential between the anode and cathode. Around 0.15% of the total produced hydrogen can be released into the atmosphere along with oxygen [1].

3) Operational purging: The hydrogen generated from the electrolyzer has contaminants like water and oxygen that require purification. Water is removed via compression drying and adsorption dryers, and when one of the adsorption units is in use, the other one undergoes regeneration. During this regenerative step, the unit is purged with hydrogen. However, depending greatly on the design, purged hydrogen might either be vented or recirculated. As a result, operational purging largely depends on the design of each individual unit, and based on the design, there may be zero or multiple sources. Nowadays, in almost all designs, the dryers use recirculating regeneration.

4) Unintended leaks from joints, flanges, and valves: Due to its smaller molecular size, hydrogen has a high tendency to leak through seals, flanges, joints, valves, etc. This is also very much dependent on the design of the unit and the type of flanges and valves used in the production unit [1], [19]. There is not much information available in the literature on the fugitive emissions of hydrogen.

The total amount of hydrogen that might enter the atmosphere is equal to the sum of the venting from the above-mentioned sources. Due to its rapid dispersion and high escape velocity, most of the hydrogen disperses and becomes diluted below its lower flammability limit as soon as it is vented. However, there is still a possibility that some small amount gets ignited as soon as it comes in contact with the air. It is assumed that 10% of hydrogen released during startups and

shutdowns will ignite before dispersing [19].

2.3. Global warming potential of hydrogen

2.3.1. Indirect global warming

The leakage of hydrogen into the atmosphere can offset some of the benefits of the green hydrogen economy. Hydrogen is not a direct greenhouse gas, however, by leaking into the atmosphere, it can reduce the tropospheric and stratospheric concentration of hydroxyl radicals($^{\cdot}OH$) by following reaction with OH: [20], [21]

$$H_2 + {}^{\cdot}OH \longrightarrow H_2O + H \tag{2.9}$$

OH radicals are the primary scavengers of gases such as methane. The reduction of hydroxyl radicals by hydrogen delays methane decomposition, resulting in a longer lifetime. Greenhouse gas like methane is mainly controlled by .OH by the given reaction: [20]

$$CH_4 + {}^{\cdot}OH \longrightarrow CH_3 + H_2O \tag{2.10}$$

The Earth absorbs energy from the sun and, according to thermodynamic laws, must emit the same amount of energy into space. However, due to the presence of greenhouse gases in the Earth's atmosphere, the Earth retains more energy than it emits. This difference is known as radiative forcing, and it causes the planet to warm [22]. As a result, emissions of hydrogen indirectly increase the radiative forcing due to greenhouse gases and contribute to global warming.

2.3.2. Global Warming Potential(GWP) metric

In order to quantify the global warming impact of any gas, the most commonly used and accepted metric is GWP. The global warming potential, or GWP, of a gas, measures the ability of a gas to trap heat in the atmosphere over a certain period of time. The effects of various gases and how they affect climate change can be compared. The standard method for calculating the impact of emissions is to compare the radiative forcing of any gas to carbon dioxide and integrate it over time. In the case of GWP-100, the time period is 100 years, and for GWP-20, it is 20 years [21].

Understanding the GWP value of hydrogen is important for assessing its potential as a low-carbon fuel source. To date, three models—by Paulot [23], Derwent [24], and the most recent one by Warwick [5]—are available to estimate the global warming potential of hydrogen. The resulting GWP-100 varies from 5(+/-)1 estimated by Derwent's model to 11(+/-)5 based on Paulot's and Warwick's models. Derwent's model yields a GWP-20 of 12, while Warwick and Paulot's models yield a GWP-20 of 33. The distinction is brought about by the fact that the climate effect is attributed to a number of different phenomena. For instance, Warwick and Paulot included the effect of ozone and water vapor in the stratosphere in their estimate of radiative forcing, whereas Derwent did not include this phenomenon in

their estimation. Derwent assumed that the methane route would contribute half as much as the tropospheric ozone, however, in Paulot's model, the methane route has a greater contribution than tropospheric ozone. Based on these models, the lifetime obtained for hydrogen is 1.5 years for Derwent's model and 2.1 years for Paulot's model. It is clear that hydrogen has a shorter lifetime in comparison to carbon dioxide, which can take hundreds of years to be removed by natural processes. Figure 2.5 shows the atmospheric mass increment for hydrogen, methane, and carbon dioxide over 100 years. According to the graph, the hydrogen mass in the atmosphere almost disappears after 20 years, whereas approximately 40% of the carbon dioxide is still left. Therefore, the GWP-20 is used to calculate the equivalent carbon dioxide emissions from the production of green hydrogen because it is thought to be a better indicator of the global warming potential of short-lived gases like hydrogen.

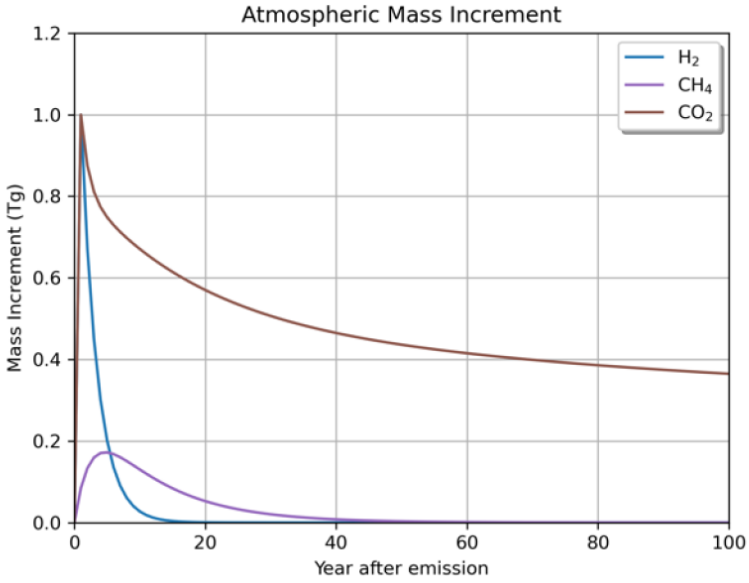

Figure 2.5: Atmospheric mass increment vs time [21]

2.3.3. Comparison with grey hydrogen

Hydrogen produced from methane using the steam methane reforming(SMR) process is known as grey hydrogen. Currently, most of the hydrogen is produced by the steam methane reforming(SMR) process. This is an energy-intensive process in which heating is used to convert methane to hydrogen. The by-product of this process is carbon dioxide and heating is mostly provided by combusting natural gas which produces more carbon dioxide. The reaction taking place is [25]:

$$CH_4 + 2\,H_2O \longrightarrow 4\,H_2 + CO_2 \tag{2.11}$$

The greenhouse gas emissions from SMR can be divided into two parts:
1) Every 4 moles of hydrogen generates 1 mole of carbon dioxide
2) The above endothermic reaction requires approximately 0.181MJ of energy to produce one mole of hydrogen which is supplied by burning natural gas. Burning natural gas for heat produces 50g of carbon dioxide per MJ of energy [26], [27].
In addition to direct emissions of carbon dioxide, some unburnt methane also ends up in the atmosphere. Approximately 3.5 wt% of total methane consumed during production leaks into the air [28]. Methane is a potent greenhouse gas with a global warming potential of 86 with respect to CO_2 over a 20-year time frame [25], [28]. To compare the global warming impact of green hydrogen with grey hydrogen, the carbon dioxide equivalent emissions from the steam methane reforming production unit are estimated and results are discussed in the section 3.4.

2.4. Green hydrogen in 2050

The deployment of renewable sources of energy is increasing globally, as is the production of hydrogen using electricity from renewable sources. Green hydrogen has a very high potential as it is directly linked to the potential of solar and wind sources, which are abundant. European policymakers aim to explore this potential and make the EU industry a leader in green hydrogen. Scaling up green hydrogen production is critical to achieving this goal [6]. The DNV Hydrogen Report 2022 [4] predicts that green hydrogen will remain expensive for the next decade, but there will be a reduction in prices by the 2030s, and by the 2050s, there will be wider use of hydrogen as an energy carrier. Europe is expected to have 111 GW of electrolyzer capacity by 2030 and 574 GW by 2050. Globally, electrolyzer capacity is expected to reach around 3075 GW by 2050. The global hydrogen production by various production routes is depicted in Figure 2.6.

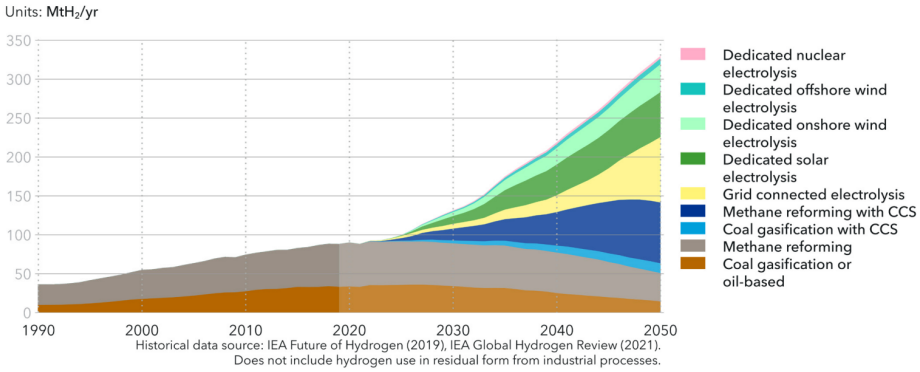

Figure 2.6: Global hydrogen production [4]

The graph makes it clear that, in addition to electrolysis, traditional methods like coal gasification and carbon capture also account for a significant portion of hydrogen production. Green hydrogen production by water electrolysis has been on the rise

since 2020 and is expected to take a major share by 2050. These forecasts show that the hydrogen industry has a bright future and has sizable growth potential in the ensuing decades. However, it also implies that analyzing the impact of hydrogen emissions is critical in the rapidly expanding green hydrogen economy.

2.5. Conclusions

This chapter discusses four different types of water electrolysis technologies. The most mature technology is alkaline water electrolysis, and PEM is the second most widely used. There are four potential sources of leakage in an electrolysis unit:

1. Venting at start-up and shutdown
2. Venting due to hydrogen cross-over
3. Operational purging
4. Unintended leaks from joints, flanges, and valves

Later in the chapter, the indirect global warming potential of hydrogen is discussed. Hydrogen can delay the decomposition of the powerful greenhouse gas methane in the atmosphere by reacting with hydroxyl radicals, which would otherwise consume methane. The global warming potential (GWP) of hydrogen could be 33 based on a 20-year period, as reported by Warwick's and Paulot's model. The future potential of green hydrogen is also discussed, with Europe expected to reach 574 GW of electrolyzer capacity by 2050, according to the DNV Hydrogen Report 2022.

3

Leakage and venting estimations

Leakage calculations are performed in this chapter. To do so, the design basis and related assumptions are first discussed. It is followed by a discussion of the methodology used to identify the primary sources of leakage, and then the obtained results are analyzed.

3.1. Basis of Design

The leakage calculations are carried out based on the available in-house data at Worley. It should be noted that the goal of these calculations is to estimate the amount of hydrogen that enters the atmosphere and determine the need for solutions to prevent it. All of the estimates are based on the following assumptions:
1) Green hydrogen is produced via low-pressure alkaline electrolysis.
2) Capacity of the unit is 100 MW with 10 electrolyzers in place.
3) Electrolyzers can be ramped down to a minimum of 15% capacity.
4) All electrolyzers are operated at equal loads.
5) Power to green hydrogen unit is provided by a dedicated offshore wind farm.
6) Power profile of the wind farm is based on the Hollandse Kust Noord (HKN) offshore wind farm (Appendix A.1).
7) Time period of the analysis is one year.
8) It takes two hours after a start-up to achieve desired purity of hydrogen.

As already stated, the calculations are based on the assumption that low-pressure alkaline electrolysis is used to produce green hydrogen. The fundamentals of the technology are explained in the section 2.1. Figure 3.1 depicts the process flow diagram of the alkaline electrolysis production plant based on the Worley design. The electrolyzer modules are filled with 30 wt% KOH solution (electrolyte), and ultra-pure demineralized water is fed into the electrolyzer. Electrical current flows through the cell stacks, where oxygen and hydrogen are formed at the electrodes. A mixture of catholyte (KOH) and hydrogen flows from the cathode to the

catholyte header tank, from which the catholyte is pumped via the catholyte filter and catholyte cooler back into the electrolyzer anode side. A mixture of anolyte and oxygen flows from the anode to the anolyte header tank, from where it is pumped via the anolyte cooler into the electrolyzer cells on the cathode side. Oxygen from the anolyte header tank enters the atmosphere via the oxygen gas coolers. The compressor unit receives the hydrogen from the catholyte header tank, which is then sent to the de-oxidizer unit where the oxygen present in the hydrogen stream is converted to water. Purified hydrogen then goes into the drying units. The final usable product is compressed hydrogen [6], [29].

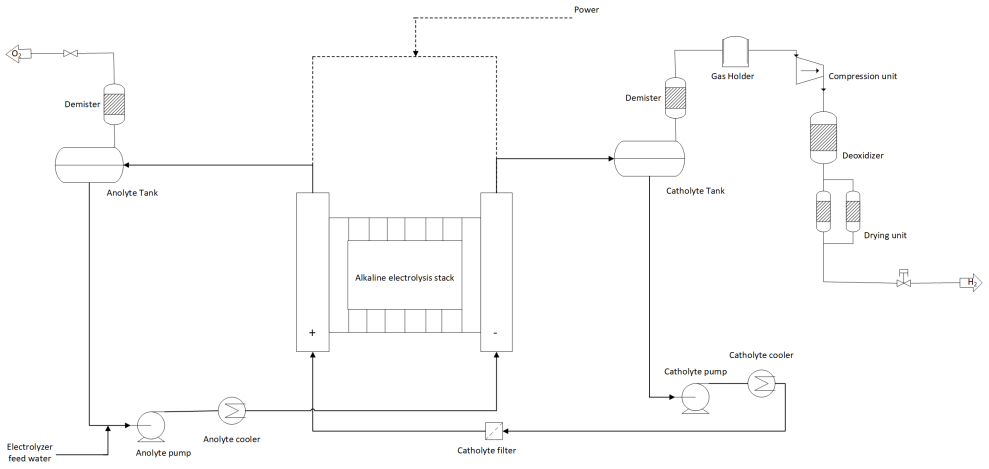

Figure 3.1: Flow diagram of alkaline electrolysis

There are four possible sources of hydrogen leakage in the electrolysis unit, which are covered in the section 2.2. The following section will go over each of these sources' estimates individually.

3.2. Estimation Methodology

The total amount of hydrogen vented to the atmosphere would be the sum of venting due to start-ups and shutdowns, hydrogen cross-over, operational purging, and leakage from flanges, valves, and seals. The methodology for estimating the hydrogen emissions from each source is described in this section.

1) Venting during start-up and shutdown: Absence of green power, scheduled maintenance, and emergencies can all cause shutdowns in an electrolysis plant. Due to the intermittent nature of offshore wind, there may be several occasions when the power available is below the minimum power required by electrolyzers to operate. In these circumstances, it is necessary to vent the hydrogen from the electrolyzer system to reduce the possibility of the formation of an explosive gas mixture. It is important to keep in mind, though, that only the electrolyzer sys-

tems are vented during these frequent shutdowns, while the compression and PDU (purification and drying unit) systems are isolated. During the shutdown, the electrolyzer system is purged and blanketed with nitrogen. After the electrolyzer system is started up at 15% capacity, produced hydrogen is vented for 2 hours to obtain the on-spec hydrogen product. This can lead to a considerable amount of hydrogen ending up in the atmosphere and is estimated using the following relationships:

*Hydrogen loss due to unavailability of power = Number of shutdowns/start-ups in one year * [Venting during single shutdown + Venting during single start-up]*

*Venting during single shutdown = Number of electrolyzer units * [Volume of the equipment involved (catholyte header tank, gas cooler, filter, and relevant piping)] * Density of hydrogen at process conditions*

*Venting during single startup = Hydrogen production rate at 15% * Number of hours hydrogen is vented after starting-up*

In addition, hydrogen is released into the atmosphere during planned maintenance and emergencies. It is assumed that complete plant failure due to any emergency occurs once every year and that entire unit maintenance is performed once every two years.

2) Venting due to hydrogen cross-over: In an electrolyzer, oxygen is produced at the anode and hydrogen at the cathode. Due to the small size of the hydrogen molecule, some amount of hydrogen passes through the membrane and ends up in the oxygen stream. The rate of hydrogen released into the atmosphere along with the oxygen stream is estimated from available in-house mass balance data.

*Hydrogen crossover = Number of hours unit is online in one year * Rate of hydrogen cross-over*

3) Operational purging: There can be two sources of operational purging in the electrolysis plant. First, hydrogen may be released into the atmosphere by qualitative analyzers found in the electrolyzer system, PDU units, and metering stations. Second, ultra-pure demineralized water is required for electrolysis. The electro-deionization unit in the ultra-pure demineralized water facility generates a small amount of hydrogen, which is then released into the atmosphere. These two sources of operational purging are continuous when the unit is operational. Based on available in-house data, operational purging is estimated as follows:

*Amount of operational purging = number of hours the unit is operational in one year * [Total number of analyzers * Rate of venting through one analyzer + Rate of venting from demin water facility]*

4) Leakage from flanges, valves, and seals: Any equipment that is pressurized has the tendency to leak, and such leaks occur mostly through flanges, valves, and seals. Such unintentional leaks are referred to as fugitive emissions. The American Petroleum Institute (API) published a compendium of greenhouse gas emissions in 2009 [30] that details various methodologies for estimating these emissions. One of the methodologies used in this project is called the 'Component-Level Average Emission Factors Approach'. As the name implies, this approach is based on the emission factors for each type of component and the quantity of that type of component present in the facility. According to API, it gives the most accurate estimation for the cases when very little or no monitoring data is available. The emission factors provided in the compendium are for methane emissions. Hydrogen has a lower viscosity and smaller molecular size compared to methane, which may lead to faster leakage rates than methane. On a molar basis, hydrogen can leak approximately three times faster than methane for a given set of conditions like pressure, hole size, etc [31]. Hydrogen leakage in valves, control valves, flanges, and pressure relief valves is estimated using the relationship shown below:

*Emissions of H_2 from all components of type A = 3 * (Molar weight of H_2/Molar weight of CH_4) * Average emission factor for the component type A * Average weight fraction of H_2 in the stream * Number of components of type A * Number of hours the unit is operational*

Apart from the block valves, control valves, flanges, and pressure-relief valves, leakage through compressor seals can also be significant. The estimation of hydrogen leakage through the compressor seals is done from available Worley in-house data. More details on leakage calculations can be found in Appendix A.2.

These estimates provide the hydrogen emissions from the green hydrogen production plant. The results of these estimations are described in the section 3.3. The fact that some of the hydrogen that has been vented could ignite at the stack's tip even before it disperses and dilutes below its lower flammability limit is also taken into account in these calculations. This value is assumed to be 10% of the vented hydrogen [19]. Obtained numbers are further quantified in the section 3.4 to estimate equivalent carbon dioxide emissions using the global warming potential (GWP-20) metric(2.3.2). Additionally, these emissions are compared to the CO_2 emissions from the grey hydrogen plant of the same capacity.

3.3. Estimation Results

The results for the hydrogen leakage from the green hydrogen unit are based on the 100 MW alkaline electrolysis unit. Figure 3.2 shows the results obtained from the calculations. The hydrogen crossover in the electrolyzer and start-ups/shutdowns brought on by a lack of power are clearly the two main sources of hydrogen leakage, as is evident from the figure 3.2. About 123.8 tons of hydrogen emissions are produced annually by a 100 MW green hydrogen unit (Appendix A). These emissions are approximately 1% of the total hydrogen produced by the unit in one year.

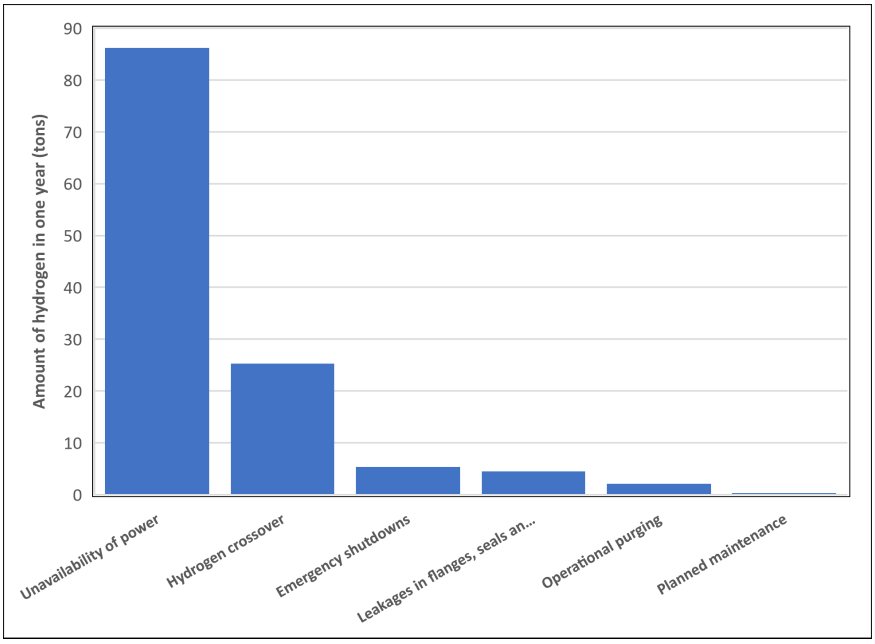

Figure 3.2: Hydrogen emissions per source from 100MW electrolysis unit

Europe is anticipated to reach a 574 GW capacity of green hydrogen from electrolysis by 2050, as mentioned in section 2.4. The total hydrogen emissions from 574 GW capacity units will be around 711 kton/year. This calculation is simplified by assuming 574 GW of electrolysis capacity would mean 5740 trains of 100 MW capacity each. In the future, when the green hydrogen economy is anticipated to play a dominant role, it is important to note that these findings are essential in determining whether hydrogen emissions can actually pose problems. These estimations are also critical to identify the areas where improvements can be made to reduce hydrogen leakage and minimize environmental impact.

3.4. Realization of hydrogen emissions

By estimating CO_2 equivalents of hydrogen emissions using the global warming potential (GWP) metric, the effect of hydrogen on global warming is quantified. The global warming potential value of 33 provided by Paulot's model is used for the calculations, as explained in section 2.3.2.

For 100 MW of capacity, 123.8 tons of hydrogen are vented to the atmosphere annually, which is equivalent to approximately 4087 tons of carbon dioxide. The annual carbon dioxide equivalent emissions from 574 GW of capacity will be 23.4 Mtons, which is approximately 84% of Denmark's total CO_2 emissions in the year 2021 [32]. The annual cost of these emissions would be approximately 1 billion

USD. This number is based on the DNV Energy Transition Outlook report from 2021 [4], which states that by 2050, the average carbon tax will level off at 50 USD (56 euros) per metric ton of CO_2. Currently, carbon is taxed in Europe at a rate of around 108 USD (100 euros) per tonne [33], amounting to 2.5 billion USD annually. In a nutshell, green hydrogen can only be the fuel of the future if there are solutions to this rising issue.

Another calculation is performed to compare GHG emissions from green and grey hydrogen plants. Every year, the electrolysis unit of 100 MW capacity produces 12.7 ktons of green hydrogen, which results in 4.09 ktons of CO_2 equivalent emissions. To produce the same amount of hydrogen with the steam methane reforming, carbon dioxide equivalents released to the atmosphere are 262.3 ktons, which is 64 times more than what a green hydrogen plant with the same capacity would emit. These two calculations describe the global warming impact of green hydrogen as well as compare grey hydrogen with green hydrogen. The comparison with grey hydrogen helps assess the environmental benefits of green hydrogen production and suggests that green hydrogen has a significantly lower global warming impact relative to grey hydrogen. The findings of this study can provide valuable insights for policymakers and industry stakeholders in making informed decisions about the adoption of green hydrogen technology.

3.5. Conclusions

This chapter discusses the primary assumptions upon which estimations are based. The estimation methodology and results obtained are also discussed in detail. These findings are further analyzed to quantify the global warming impact of green hydrogen. This chapter highlights the following main points:

- The two biggest contributors to hydrogen emissions from the green hydrogen alkaline electrolysis unit are frequent shutdowns and startups due to the lack of renewable power, and the hydrogen crossover in the electrolyzer.
- By 2050, Europe's electrolyzer capacity is predicted to be 574 MW, resulting in carbon dioxide equivalent emissions of 23.4 Mtons/year, or about 84 percent of Denmark's 2021 total CO_2 emissions. Based on the current carbon tax of 108 USD (or 100 euros) per tonne, these emissions would cost about 2.5 billion USD annually.
- The carbon dioxide equivalent emissions from grey hydrogen production plants are approximately 64 times higher than those from green hydrogen plants of the same production capacity.

This chapter demonstrates that green hydrogen is the solution to achieve energy transition over grey hydrogen. But it also establishes the need for investigating the ways to reduce hydrogen emissions in order to reach net zero emissions by 2050.

4

Solutions to hydrogen emissions

In chapter 3, hydrogen emissions from electrolysis plant are estimated and the results are discussed. The analysis has determined the necessity of investigating potential ways to lower hydrogen emissions. The two biggest contributors to hydrogen emissions in an electrolysis production unit are startups/shutdowns due to power shortages and hydrogen crossover in the electrolyzer.
The following three potential solutions are explored in this project:

1) Flaring System - Vented hydrogen can be combusted at the tip of the flaring system. Hydrogen emissions from start-ups and shutdowns brought on by lack of power and maintenance can be reduced by installing a flaring system on the hydrogen vent stack. Designing a flare is out of the scope of this project. However, the combustion of hydrogen in the presence of air may produce a significant amount of nitrogen oxides (NOx). To evaluate the viability of this solution, NOx emissions that are produced during flaring are estimated.

2) De-hydro reactor - The second biggest contributor to hydrogen emissions is the hydrogen cross-over from the cathode to the anode side of the electrolyzer which ends up in the oxygen product stream. The catalytic recombination of hydrogen with oxygen in a packed bed reactor is investigated to prevent hydrogen emission due to crossover. The reactor is modeled in MATLAB, and the reactor's financial feasibility is also examined.

3) Battery energy storage system - Short-duration shutdowns caused by power outages can be minimized by installing a battery storage system. A model in MATLAB is built to obtain the optimized capacity of the system by minimizing the system's overall costs.
Each solution is discussed in detail in this chapter.

4.1. Flaring system

The combustion of hydrogen occurs more quickly than that of methane or natural gas because of the low ignition energy and high flame propagation speed of hydrogen[34]. The expansion of the flame from the point of ignition is measured by the flame propagation speed. Rapid combustion leads to localized heating and elevated temperatures, which together contribute to high adiabatic flame temperatures. The temperature attained when the products are heated by all of the heat released during the combustion reaction is known as the adiabatic flame temperature. It is primarily determined by the heating value of combustion enthalpy. Regions with temperatures higher than 1371 °C are conducive to the formation of nitrogen oxides [34].

Nitric oxide (NO) and nitrogen dioxide (NO_2), which make up nitrogen oxides, can have adverse effects on human health as well as vegetation. Humans who are exposed to high NOx levels may develop lung and respiratory infections. In plants, it can harm plant foliage and lower crop productivity. They also increase air pollution. Smog, which is most noticeable as a brown haze, is caused by NOx gases and is more prevalent during the summer. Acid rain is also a result of NOx gases' formation of nitric acid. Additionally, NOx buildup in oceans causes harmful algae to bloom, which has a negative effect on aquatic life[35]. In order to determine whether the solution is feasible, NOx emissions must be carefully examined.

4.1.1. Methodology

Conventionally, NOx emissions from natural gas flares are estimated by multiplying the activity rate by emission factors obtained from Environmental Protection Agency(EPA) [36]. The emission factor from EPA is the constant value of $2.92*10^{-5}$ of NOx per MJ of LHV of gases sent to flare. The activity rate is calculated by multiplying the volume of gas sent to the flare by its lower heating value (LHV). The emission factor specified by EPA is based on the flaring of natural gas, which has lower NOx emissions than hydrogen due to its lower adiabatic flame temperature [37]. Data from the literature [38] is used to determine the relationship between NOx emissions and adiabatic flame temperature. Figure 4.1 shows the fitted curve and a cubic relationship between NOx emissions and adiabatic flame temperature. The following correlation is used to estimate the NOx emissions for hydrogen burning:

*NOx emissions = Emission factor * Amount of H_2 sent to flare * LHV of H_2 * (Adiabatic flame temp of H_2/Adiabatic flame temp of CH_4)^3*

The stoichiometric combustion reaction of pure H_2 and CH_4 would be: [34]

$$2\,H_2 + (O_2 + 3.76\,N_2) \longrightarrow 2\,H_2O(g) + 3.76\,N_2 \tag{4.1}$$

$$CH_4 + 2\,(O_2 + 3.76\,N_2) \longrightarrow CO_2 + 2\,H_2O(g) + 7.52\,N_2 \tag{4.2}$$

Respective heats of formation are taken from Perry's Handbook [39]. Adiabatic flame temperature of hydrogen and methane is estimated using the following rela-

tions of heat capacities:[39]

$$Cp(H_2O) = 4.184(8.22 + 0.00015T)$$

$$Cp(N_2) = 4.184(6.5 + 0.001T)$$

$$Cp(CO_2) = 4.184(10.34 + 0.00274T - 195500/(T^2)$$

Adiabatic flame temperature is reached when the enthalpy of reactants and products is equal.

$$\Sigma H_{\text{reactants}} = \Sigma H_{\text{products}}$$

$$H = Moles_{\text{stoichiometry}} * C_{\text{p}}(J/mole \cdot K) * \Delta T(K)$$

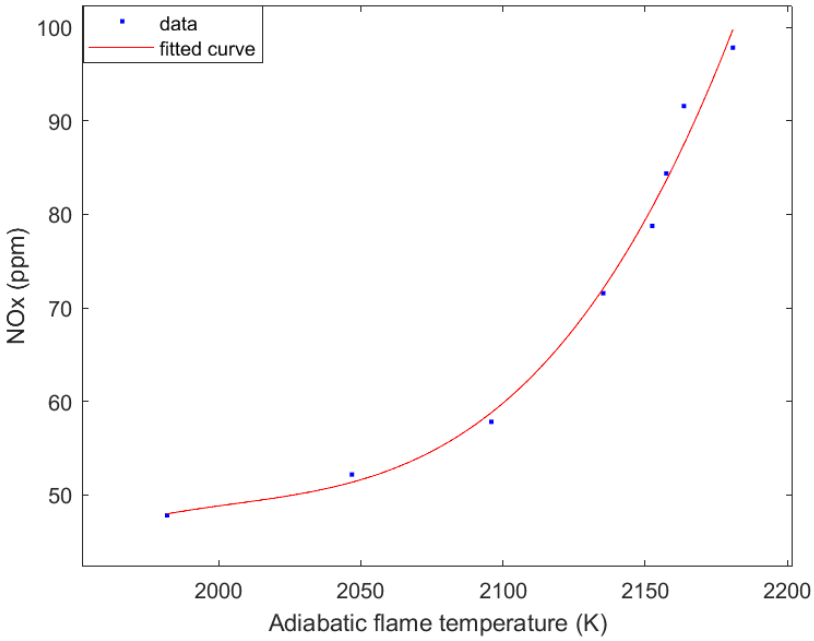

Figure 4.1: NOx vs adiabatic flame temperature

4.1.2. NOx emission results and discussion

The resulting adiabatic flame temperature of the hydrogen is 2481°C and of methane is 2161°C, which is significantly lower than hydrogen as explained in the section 4.1.1. Higher flame temperatures of hydrogen may lead to higher NOx emissions. The hydrogen vented during startups and shutdowns of the green hydrogen unit, which has a 100 MW capacity, is approximately 92 tons/year and if it is flared, the estimated annual NOx emissions are 467.6 kg. The resulting emissions are approximately 2% of the NOx emissions that would have been produced when the same amount of hydrogen is produced from methane by steam methane reforming. The NOx figures for the grey hydrogen plant are based on the in-house estimations for clients. Flaring hydrogen is a viable solution as it will address the issue of hydrogen emissions, and NOx emissions are considerably lower than grey hydrogen units.

Several companies provide Ultra-Low Emissions flares, such as enclosed flares, which can reduce NOx emissions produced during hydrogen flaring. Emissions are reduced by precisely controlling the amount of air mixed with the gas in a premixed chamber, which lowers the flame temperature and thus NOx emissions [40]. Other technologies such as steam injection can also be incorporated during flaring, steam injection provides a cooling effect and also lowers the flame temperature and, as a result, NOx production [34]. However, the steam injection could be costly, and steam availability in a green hydrogen plant is extremely limited. Such methods could reduce NOx emissions, but they are typically used for natural gas flaring and should be investigated for hydrogen flaring. However, it is important to note that flaring should only be considered as a temporary solution until a more long-term solution, such as a battery storage system to reduce the frequency of shutdowns and startups and, consequently, the amount of hydrogen vented, can be implemented.

4.2. De-hydro reactor

Catalytic recombination of oxygen and hydrogen in the oxygen product stream could be an option to prevent hydrogen emissions from hydrogen crossover in the electrolyzer. The following reaction takes place:

$$H_2 + \frac{1}{2} O_2 \longrightarrow H_2O \tag{4.3}$$

The heat of reaction of this exothermic reaction is 241.8 kJ/mol. The MATLAB program is used to model and optimize the reactor for this recombination reaction. A de-hydro packed bed reactor is modeled using the intrinsic kinetic data published in open literature [41]. The reaction takes place in the presence of 0.5 wt% Pd catalyst on a special alumina surface. The effect of reactor inlet conditions like temperature and pressure is also analyzed on overall conversion along the length of the reactor. Later, the economic feasibility of a few potential designs is compared by calculating the capital and operating costs of each design. Finally, the optimal design is selected based on its performance and economic viability.

4.2.1. Modeling of reactor

Fixed-bed reactor models can be classified into pseudo-homogeneous and pseudo-heterogeneous. Pseudo-homogeneous models assume thermal and concentration equilibrium between the bulk fluid phase and the catalyst phase, whereas heterogeneous models consider mass and heat transfer between the bulk of the fluid and the catalyst phase. Based on the mixing in one or two dimensions in the reactor, models can be one-dimensional or two-dimensional. Two-dimensional models take into account mixing in two directions while one-dimensional models assume that the reactor is perfectly mixed in one direction [42]. This reactor model is one-dimensional and based on the following assumptions:

1. Packed bed reactor is modeled using the simple one-dimensional heterogeneous model and assumes plug flow.
2. Adiabatic and steady-state conditions exist. Therefore, no external cooling or heating in the reactor.
3. Catalyst weight is uniformly distributed over the length of the reactor.
4. Catalyst particles are spherical.
5. Activity of the catalyst is constant.
6. Reactant is assumed to be diffusing through a hypothetical film near the catalyst from the bulk of the fluid to the surface of the catalyst.
7. Reaction occurs instantaneously on the surface of the catalyst as soon as mass transfer from the bulk fluid takes place.

The model uses following equations: [41], [42]

Fluid phase:

$$u_s \frac{dC}{dz} = k_f * a * (C - C_s)$$

$$u_s * \rho_f * C_p * \frac{dT}{dz} = h_f * a * (T_s - T)$$

Solid phase:

$$k_f * a * (C - C_s) = -R_v$$

$$h_f * a * (T_s - T) = -R_v * (-\Delta H_r)$$

Pressure drop- Ergun's equation

$$f = \frac{(1-\epsilon)}{\epsilon^3}(1.75 + 150\frac{(1-\epsilon)}{Re_p})$$

$$\frac{dP}{dz} = \frac{-f * \rho_f * {u_s}^2}{Re_p}$$

where

$$a = \frac{6(1-\epsilon)}{d_p}$$

for $d_p/D<0.5$

$$\epsilon = 0.4 + 0.05(d_p/D) + 0.412(d_p/D)^2$$

According to the data sheet provided by the catalyst vendor, BASF, catalyst particle diameter (d_p) ranges from 2-4 mm and is assumed to be 4 mm in this study. The order of reaction with respect to hydrogen is assumed to be one due to the presence of oxygen in excess. Rate of reaction based on unit volume of reactor:

$$-R_v = \eta * k * C_s$$

η is the catalyst effectiveness factor which is assumed to be 0.92 based on the literature [41].

$$k = 5.37 * 10^{11} * exp(-76420/RT)$$

As the reaction is assumed to occur instantaneously on the external surface of the catalyst particle, Frossling correlation is used to estimate mass transfer coefficient:[43]

$$Sh = 2 + 0.55 * {Re_p}^{0.5} * Sc^{0.33}$$

Correlations for thermodynamic properties like specific heat capacity and viscosity listed in table 4.1 are taken from Perry's Handbook [39]:

Table 4.1: Physical properties for various components [39]

Component	Property	Correlation used
H_2	μ (kg/m·s)	$1.797*10^{-7} * T^{0.685}/(1 - 0.59/T) + 140/T^2$
	C_p(J/mol·K)	4.184*(6.62 + 0.00081*T)
O_2	μ (kg/m·s)	$2.41*10^{-7} * (M_{O2} * T)^{0.5}$
	C_p(J/mol·K)	4.184*(8.27 + 0.000258*T - 187700/T^2)
H_2O	μ (kg/m·s)	$1.7096*10^{-8} * T^{1.1146}$
	C_p(J/mol·K)	4.184*(8.22 + 0.00015*T)

The following three ordinary differential equations are solved in MATLAB using the Runge-Kutta method with the Ode15s solver.

$$\frac{dC}{dz} = -\frac{C * k * k_f}{u_s * (k_f * a + k)}$$

$$\frac{dT}{dz} = \frac{(k * k_f * a * C) * (-\Delta H_r)}{(u_s * C_p * \rho_f) * (k_f * a + k)}$$

$$\frac{dP}{dz} = \frac{-f * \rho_f * {u_s}^2}{Re_p}$$

The following boundary conditions are provided to solve the ODEs:
$C(z=0) = C_{H_2 in}$
$T(z=0) = T_{in}$
$P(z=0) = P_{in}$

4.2.2. Base case and optimization

The parameters chosen for the base case are taken from the specifications of the oxygen stream of a 100 MW low-pressure alkaline electrolysis unit. Inputs are the inlet temperature, pressure, and composition of the stream. Initial guesses for the reactor geometry (length and diameter of the reactor) are provided. For the purpose of analyzing reactor performance in various scenarios, the base case serves as a point of reference. The following baseline parameters are used to optimize reactor length and diameter:

Table 4.2: Base case parameters

	Unit	
Inlet temperature	°C	50
Inlet pressure	kPa	130
Inlet flow rate	t/h	16.4
Mole% of inlet water-saturated stream		
y_H_2	%	0.4
y_H_2O	%	9.5
y_O_2	%	90.1

The Fmincon function in MATLAB is used to carry out optimization. The objective of the optimization is to minimize the concentration of hydrogen in the oxygen product stream. Reactor geometry is limited to achieve conversion of hydrogen to 99.8% and the pressure drop across the reactor should not exceed 15 kPa. The pressure drop constraint is set based on the in-house operational experience. The algorithm used to optimize the reactor geometry for given process conditions is captured in Figure 4.2.

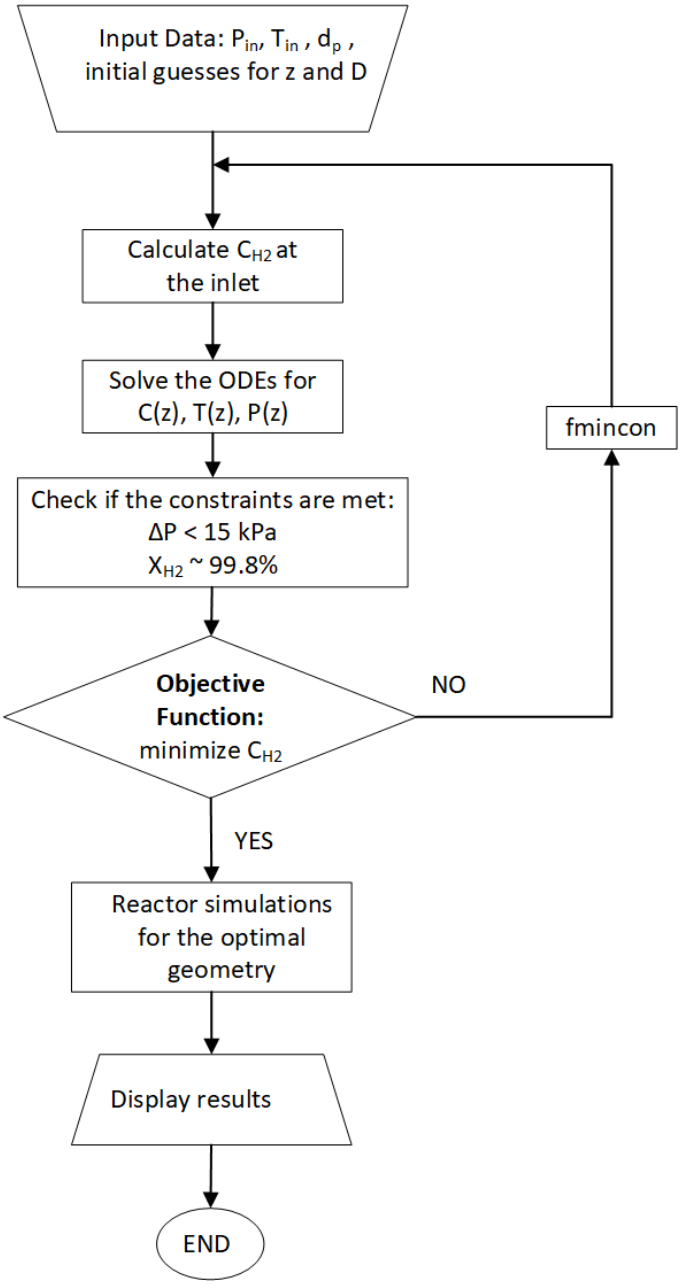

Figure 4.2: Algorithm of reactor optimization

Figure 4.3 displays the results for the base case. The optimized diameter is 2.45 m, and the optimal length obtained is 2.97 m. The trends show that the reactor model

performs as expected. As the conversion increases along the length of the reactor, the hydrogen concentration in the bulk fluid decreases. The reaction is exothermic due to which the temperature rises in an adiabatic reactor along its length. The pressure drop over the reactor is approximately 11 kPa, which complies with the established constraints. As the pressure decreases along the length, the volumetric rate increases, resulting in an additional decrease in reactant concentration on top of the decrease caused by the conversion. The rate of the reaction decreases as the reactant concentration decreases. As a result, if the reactor diameter is too small, there will be greater pressure drops in the reactor, leading to lower reaction rates and longer reactors for the same conversion. On the other hand, if the reactor diameter is too large, it may result in lower reactor pressure drops but more catalyst may be needed. Consequently, choosing the right reactor geometry is essential for achieving the best conversion and an economically optimal design.

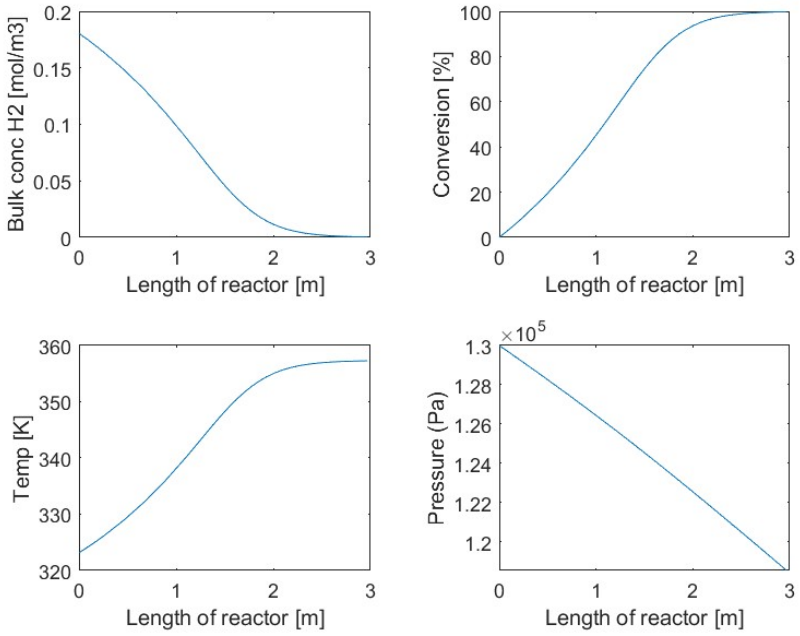

Figure 4.3: Results of base case

In the section 4.3.4, the impact of changing inlet parameters like temperature and pressure is further examined in order to determine the validity of the results and the reactor model. The robustness of the reactor model and its ability to precisely forecast the behavior of the system under various operating conditions are both assessed using this sensitivity analysis.

4.2.3. Sensitivity Analysis

Inlet temperature and pressure are varied for the base case reactor geometry, and the behavior in the reactor is examined. As shown in figure 4.4, raising the inlet temperature can speed up the reaction because of faster kinetics, which leads to full conversion more rapidly. The reaction reaches completion in almost 0.5 m when the inlet temperature is increased to 383 K/110 °C. However, increasing the temperature in an exothermic reaction is limited by material handling costs.

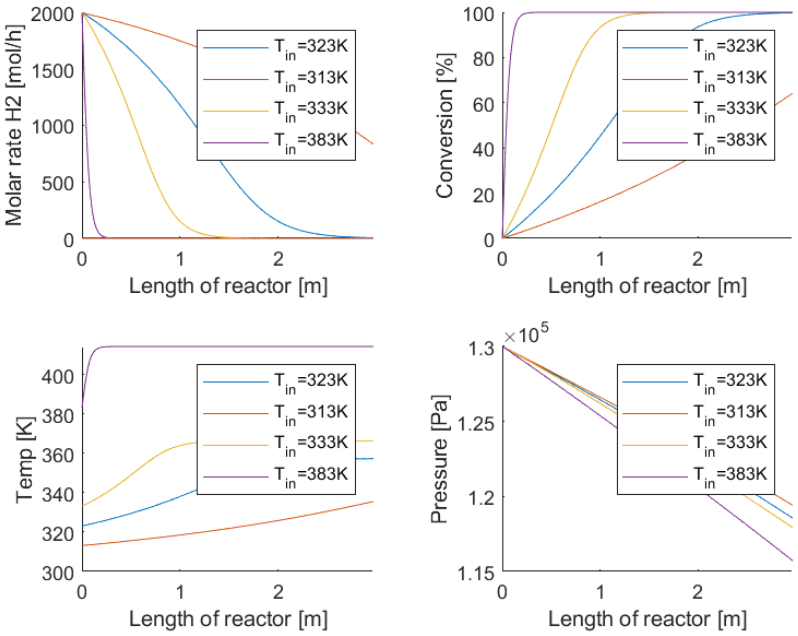

Figure 4.4: Effect of inlet temperature on reactor model

Increasing the inlet pressure is anticipated to increase conversion. The same result is depicted in figure 4.5. At an inlet pressure of 1030 kPa, the reaction reaches complete conversion in approximately 0.5 m, whereas, it takes around 3 m at 130 kPa. This is due to the fact that when the reactants are gaseous, increasing the pressure causes both an increase in the amount of reactant per unit volume and the frequency of molecule collisions. This increases the rate of reaction, and the reaction reaches completion faster. Moreover, pressure drop in the reactor becomes less significant at higher inlet pressures. The effect of changing the inlet temperature and pressure on model results is as expected, indicating that the model accurately predicts the behavior of the de-hydro reactor.

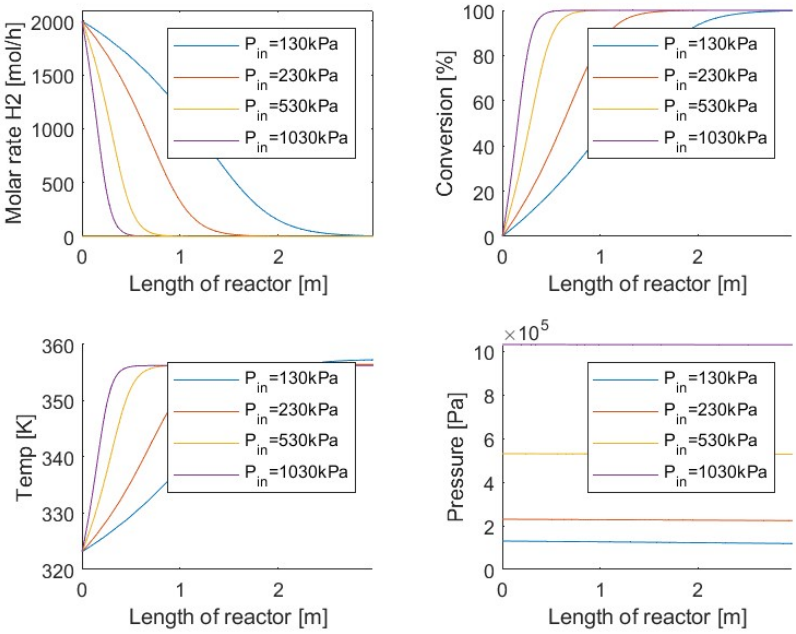

Figure 4.5: Effect of inlet pressure on reactor model

4.2.4. Model Validation

As stated in the section 4.2.1, physical properties such as specific heat capacity and viscosity are estimated using correlations obtained from Perry's Handbook [39]. These estimates are verified by comparing them to the properties obtained from UNISIM simulations of the respective process streams. The available vendor data sheet of the commercial de-oxidizer reactor is used to validate the reactor model further. The optimized reactor geometry estimated from the reactor model matches the vendor data sheet by 98.5% for the specific de-oxidizer reactor. The datasheet states that a catalyst bed of 1 m diameter and 1.3 m length can achieve 99.8% conversion, and the reactor model estimates the diameter to be 1 m and the length to be 1.32 m for the same set of inlet parameters. The model's estimates of exotherm and pressure drop in the reactor are also within the limits specified in the document. This validation increases the credibility of the reactor model and demonstrates its reliability for further analysis of the feasibility of the solution to the hydrogen crossover issue. More details are available in Appendix B.

4.2.5. Issues in alkaline electrolysis unit

This section discusses the potential issues that may arise if the de-hydro reactor solution is implemented in an alkaline electrolysis unit. The electrolyte used in al-

kaline electrolyzers is aqueous and contains 30% by weight of KOH, as mentioned in the section 3.1. The main problem is that the electrolyte, KOH, entrains with the oxygen and hydrogen product streams from the electrolyzers. The catalyst of the de-hydro reactor uses the precious metal Palladium and is very expensive. According to catalyst vendor BASF, KOH can poison the palladium catalyst and must be removed to ppb levels to prevent catalyst poisoning. The catalyst's high sensitivity to KOH can reduce its lifespan from 15-20 years to just 5 years. KOH should be reduced to less than 100 $\mu g/Nm^3$, as also reported by the catalyst vendor. Therefore, it is critical that KOH be scrubbed before being sent to the de-hydro reactor. One possibility could be to incorporate a scrubber that uses water to remove entrained KOH droplets from the gas stream. However, due to the low operating pressures in the low-pressure alkaline system, adding additional equipment such as a scrubber followed by a reactor would necessitate at least single-stage compression. Another possibility could be that if the oxygen stream is compressed, with each compression stage, it not only removes water but also knocks out the KOH in such a way that the outlet of the third stage is reported to be down to acceptable levels to prevent catalyst poisoning. Based on this information, three designs are proposed and discussed in the section 4.2.6.

4.2.6. Proposed Designs

In order to prevent hydrogen emissions from the cross-over, the following three designs are proposed. UNISIM R490 simulation software is used to simulate each of the suggested designs. The saturated gas stream to be treated has the same specifications as the base case parameters listed in table 4.2. The process conditions of the proposed designs are discussed in this section.

1) Single-stage compression followed by scrubber and de-hydro reactor: The saturated gas stream is compressed via single-stage compression. As discussed in the section 4.3.4, higher inlet pressure accelerates the reaction's rate and, hence, requires smaller catalyst beds, making the process more cost-effective. Therefore, the maximum pressure that can be attained in single-stage compression is limited by the temperature of the compressor outlet. The temperature limit is based on the API 618 design code for compressors [44] as well as the vendor's experience to ensure the compressor's adequate life. API 618 specifies a limit of 150°C for all gas services using oil-lubricated compressors, but because lubrication oils cannot be used in high-purity oxygen compression due to flammability issues, maximum temperature limits should be lower. It could go up to 140°C. In this study, the compression ratio is chosen to keep the temperature of the compression discharge below 135 °C. Accordingly, the inlet gas stream is compressed to 280.8 kPa and sent to the scrubber to remove KOH with water. De-mineralized water flows from the top of the scrubber, and gas flows counter-currently from the bottom. 90% of the water stream is re-circulated back to the top via a de-mineralized water pump and 10% of the stream is purged to prevent the accumulation of KOH. A make-up stream of fresh de-mineralized water is added to maintain a constant flow rate of water in the scrubbing column. To ensure proper wetting in the column, the total

flow rate of water into the column is 4379 kg/hr. The flow rate of water and pressure drop in the column are based on the design of the scrubber, which is discussed in detail in the section 4.2.7.1. A scrubbed gas stream at 72.5 °C and 279 kPa is sent to the de-hydro reactor. Figure 4.6 shows the process flow diagram of the design 1 simulation in UNISIM.

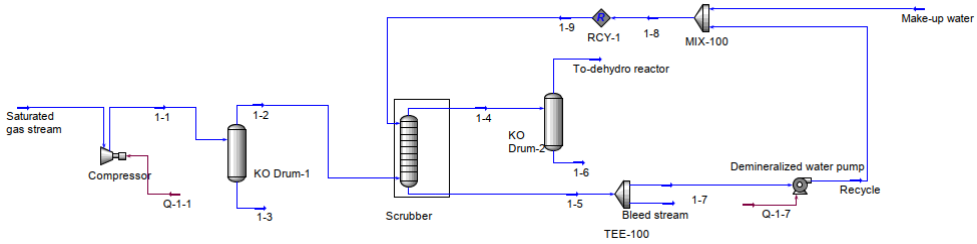

Figure 4.6: PFD: De-hydro compression design 1

2) Single stage compression followed by scrubber, heater and de-hydro reactor: The process flow of Design 2 is captured in Figure 4.7 and the process specifications upstream of the heater are the same as in Design 1. The outlet of the scrubber at 72.5 °C and 279 kPa is heated to 130 °C via an electric heater. Heating of the scrubber outlet is proposed because kinetics are faster at higher temperatures; this can reduce the catalyst requirement at the expense of an electric heater and offer a competitive design. The heater outlet temperature is determined by the in-house experience gained from handling the catalyst and material of the de-oxidizer reactor for purifying the hydrogen stream. The heated stream is then routed to the de-hydro reactor.

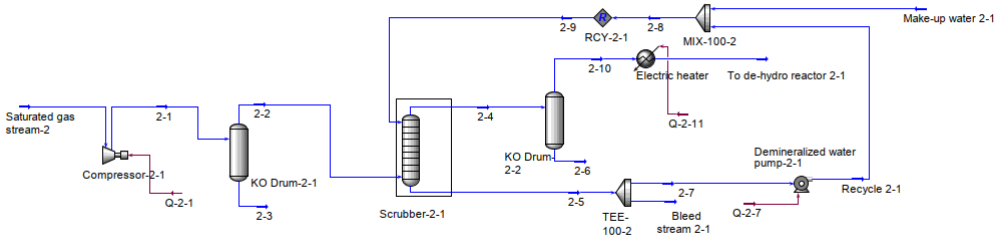

Figure 4.7: PFD: De-hydro compression design 2

3) Three stages of compression followed by de-hydro reactor: As previously mentioned, it is acceptable to send the process gas directly to the reactor after three stages of compression. The compression ratios of each compression stage

are chosen to keep the outlet temperatures below 135 °C. The inter-stage cooling is achieved using cooling water. The outlet of the third stage at 1276 kPa and 130 °C is sent to the de-hydro reactor.

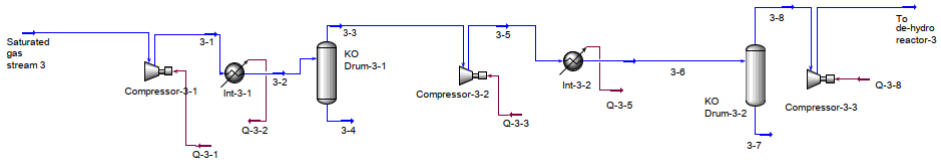

Figure 4.8: PFD: De-hydro compression design 3

4

4.2.7. Equipment Sizing

The costs of the three proposed designs are compared to determine the economic feasibility of these solutions. For the purpose of estimating the costs of the designs, each equipment is sized. Sizing criteria and results for each equipment are discussed in this section.

4.2.7.1. Sizing Criteria

Compressor and electric equipment

When higher compression ratios (discharge to suction) are required, reciprocating compressors are used for compression because they are more adaptable to changing pressures than centrifugal compressors. The energy required for the compression is obtained from the UNISIM simulations. The motor size of the reciprocating compressor is estimated based on the given relation. However, it should be noted that industrial experience with oxygen compression is very limited. As a result, the simulation predictions and the actual compressor selection can differ significantly.

*Available motor size >= 1.1*Energy required (kW)*

The standard kW ratings of the electric motors serve as the basis for the available motor sizes [45].

Other electric equipment like a de-mineralized water pump and an electric heater, are also sized the same way as a compressor. UNISIM process simulations are used to determine the energy requirements for these equipment as well.

Inter-coolers

UNISIM heat exchanger design software is used to size compressor intercoolers. They are shell-and-tube heat exchangers, with process gas on the shell side and cooling water on the tube side. Condensing process fluid is easier to accommodate on the shell side because the shell side has a larger cross-section and consequently lower pressure drops. Additionally, cooling water can be corrosive, and tube bundles are easier to clean. In case replacement is required, tube bundles are cheaper to replace relative to the exchanger shell. Exchangers are designed to have a pressure drop of no more than 0.05 bar.

Scrubber
A scrubber is required only in designs 1 and 2. Water is used for washing off KOH droplets from the process gas stream. Packed columns are most commonly used for scrubbing, particularly in the handling of corrosive liquids. The liquid flows down the column over the surface of the packing, while the gas stream goes up the column. The performance of the scrubber depends largely on the distribution of gas and liquid throughout the column. The wetting rate is an important parameter to ensure proper distribution, and it should be greater than the minimum value recommended by the packing manufacturer [46]. The ratio of volumetric liquid rate per unit cross-sectional area to packing surface area per unit volume is defined as the wetting rate. As per literature [47], wetting rates should range from $0.35*10^{-3}$ to $1.4*10^{-3}$ $m^3\ s^{-1}/m^2$ for random packing and $0.07*10^{-3}$ to $0.14*10^{-3}$ $m^3\ s^{-1}/m^2$ for structured packing.

The choice of packing is yet another crucial factor that significantly affects column performance [47], [48]. Packing should provide a large surface area, low gas flow resistance, and enough gas-liquid contact for scrubbing. Based on the geometry, packing can be classified as structured or random packing. Structured packings have a regular geometry such as stacked rings, grids, and so on, whereas random packings are dumped into the column and can take up any random arrangement such as pall rings, saddles, etc [46]. Random packings are a cheaper choice and are easier to maintain. In this project, metallic pall rings are used for KOH scrubbing because strong alkalis like KOH can corrode ceramic packings and plastic packings can only be used at moderate temperatures below 100°C [49]. Moreover, pall rings are more efficient than the most commonly used raschig rings. The packing size of 50 mm is selected because it is the best compromise between performance and cost. Smaller sizes have lower pressure drops, a larger surface area, and better gas-liquid contact, but they are significantly more expensive. However, above 50 mm, the lower price per cubic meter does not compensate for the decreased mass transfer efficiency and higher pressure drop. Therefore, sizes larger than 50 mm in a column can cause poor liquid distribution and, hence, poor separation in the column [47].

Flooding is another critical phenomenon that determines the maximum amount of vapor and liquid that a packed column can handle. Flooding can occur when the vapor velocity is extremely high, causing the drag force to exceed the force of gravity and the liquid to stop flowing down the column. The column is designed to handle 70% to 80% of the flooding gas velocity and has a gas pressure drop limit of 200-4000 Pa/m packing length [50]. The SULCOL vessel sizing tool by packing vendor Sulzer [51] is used to calculate the diameter and height of the packing of the column based on three design criteria: wetting rate, pressure drop, and flooding.

A packed column is a cylindrical vessel with top and bottom heads. The vessel shell's construction material is considered to be stainless steel 316L. Apart from a

packed bed of 50 mm metallic pall rings, the vessel shell contains packing support, distributors, and distributor support. The SULCOL tool is used to estimate the scrubber's internal diameter and packing height; however, tangent to tangent length is based on liquid holdup and minimum clearance requirements between internals in a scrubbing vessel, as shown in the figure 4.9. These minimum clearance values are adapted based on Worley's in-house experience. To estimate costs, shell thickness, and weight are calculated using an internal calculation tool based on AS1210-1997/1998 SAA Unfired Pressure Vessel Code [52]. The weight of the packing is calculated as follows:

*Packing weight (kg) = Volume of packed bed(m^3) * Packing factor(m^{-1}) * Density of packing(kg/m^3) * Packing surface area(m^2/m^3)*

For 50mm metallic pall rings, values of packing factor, packing surface area and density are 66 m^{-1}, 102 m^2/m^3) and 353 kg/m^3 respectively [47].

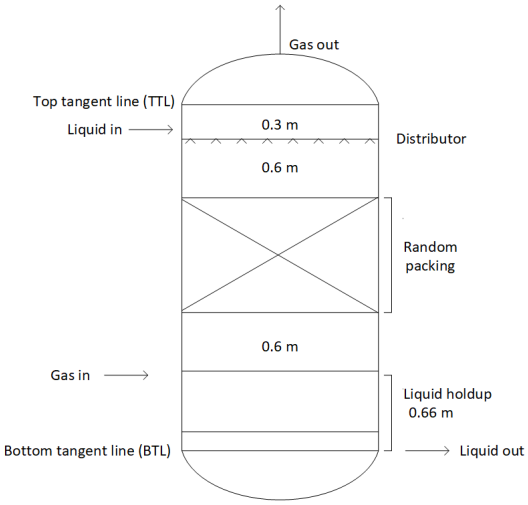

Figure 4.9: Scrubber

De-hydro reactor

The reactor vessel is also made of stainless steel 316L. The catalyst bed, catalyst support, distributors, and distributor support make up the reactor internals. Other layers, such as ceramic balls and an absorbent guard layer, are used to shield the catalyst from foreign particles. Figure 4.10 depicts a schematic of the de-hydro reactor. The mass of the reactor shell is calculated using the same tool that is used to estimate the mass of the scrubber shell. The dimensions of the catalyst bed are calculated using the model described in section 4.2.

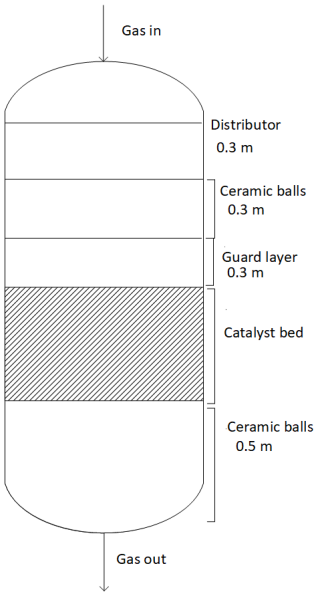

Figure 4.10: De-hydro reactor

4.2.7.2. Sizing Results

In the tables 4.3, 4.4 and 4.5, the findings of the equipment sizing for each suggested design are presented. These are further used in the section 4.2.8 to calculate the total cost of each proposed design. This information is critical in determining the most optimal design.
L is the total vessel height, D is the shell diameter and W is the weight of the vessel.

Table 4.3: Equipment sizing results of De-hydro Design-1 (PFD:Fig 4.6)

Design - 1	
Equipment	**Sizing**
Compressor	Motor size = 450 kW
KO Drum-1	L= 2 m, D = 2.29 m, W = 1.84 tons
Scrubber	L= 4.71 m, D = 1.22 m, W = 1.14 tons
KO Drum -2	L= 2 m, D = 2.13 m, W = 1.66 tons
De-hydro reactor	L= 2.57 m, D = 1.6 m, W = 1.12 tons

Table 4.4: Equipment sizing results of De-hydro Design-2 (PFD:Fig 4.7)

Design - 2	
Equipment	**Sizing**
Compressor-2-1	Motor size = 450 kW
KO Drum-2-1	L= 2 m, D = 2.29 m, W = 1.84 tons
Scrubber-2-1	L= 4.71 m, D = 1.22 m, W = 1.14 tons
KO Drum -2-2	L= 2 m, D = 2.13 m, W = 1.66 tons
Electric heater	Duty = 297.7 kW
De-hydro reactor-2-1	L= 1.95 m, D = 1.37 m, W = 0.77 tons

Table 4.5: Equipment sizing results of De-hydro Design-3 (PFD:Fig 4.8)

Design - 3	
Equipment	**Sizing**
Compressor-3-1	Motor size = 450 kW
Intercooler (Int-3-1)	Effective area = 32.1 m
KO Drum-3-1	L= 2 m, D = 2.13 m, W = 1.66 tons
Compressor-3-2	Motor size = 400 kW
Intercooler (Int-3-2)	Effective area = 20.9 m
KO Drum -3-2	L= 1.9 m, D = 1.52 m, W = 1.17 tons
Compressor-3-3	Motor size = 400 kW
De-hydro reactor-3	L= 2.1 m, D = 0.93 m, W = 0.7 tons

4.2.8. Economic Analysis

Economic analysis is performed to determine the economic feasibility of the various designs proposed to prevent hydrogen emissions from cross-over in the electrolyzers. The annualized cost for each design is calculated by estimating annual capital expenditure (CAPEX) and operational expenditure (OPEX). The economic analysis is based on prices in 2022. As a result, CEPCI (Chemical Engineering Plant Cost Index) [53] is used to perform the necessary price and cost conversions. The exchange rate of 1 euro to 1.08 USD is adopted.

4.2.8.1. CAPEX

CAPEX is calculated by multiplying the capital recovery factor by the total capital investment (TCI) [54]. Total capital investment has two major components: direct costs and indirect costs. Direct costs primarily include the costs of equipment procurement, installation, fabrication, and transportation. Overhead expenses such as insurance, security, and licensing are part of indirect costs. Direct costs are estimated by the product of lang factors and procurement cost of each equipment. The

lang factors and correlations for each equipment's procurement cost are shown in table 4.6. Indirect costs are assumed to be 40% of direct costs [54], [55]. Capital recovery factor (C_{ref}) is defined as:

$$C_{\text{ref}} = \frac{Z * (1+Z)^t}{(1-Z)^t - 1} \tag{4.4}$$

Annual interest rate(Z) is assumed to be 7% and a project lifetime(t) of 20 years.

$$TCI = Direct\ Costs + Indirect\ Costs$$
$$CAPEX = C_{ref} * TCI$$

The equipment procurement cost correlations, listed in table 4.6, are based on vendor experience, and used for Worley in-house cost estimations.

Table 4.6: Equipment procurement costs and lang factors

Equipment	Equipment procurement cost (USD)	Lang factors
Compressor	a × (Motor size (kW))^b	c
Knockout drum	d × Vessel Weight(tons)	e
Shell & tube heat exchanger	f × Effective area (m^2)	g
Scrubber	h × Vessel Weight(tons) + Cost of internals	i
De-mineralized water pump	j × Pump Weight(tons)	k
Electric heater	l × (Design duty(kW)^m	3
De-hydro reactor	n × Reactor Weight(tons) + Cost of internals	o

Obtained from Worley in-house data - confidential

The procurement costs of electric equipment such as compressors and heaters listed in table 4.6 are confidential therefore, coefficients are not shown in the table. These estimations are based on energy requirements obtained from UNISIM simulations, as discussed previously in the section 4.2.7.1. The cost of a de-mineralized water pump on the other hand, is expressed in terms of weight and is estimated based on actual pump data from vendors for varying motor sizes.
The section 4.2.7, discusses sizing and vessel weight calculations to estimate the procurement costs of other equipment. Internals costs in the scrubber and reactor can also make a significant contribution to total equipment costs. The relationships used to evaluate the cost of the internals are shown in Table 4.7.

Table 4.7: Cost of reactor and scrubber internals

Internal type	Cost (USD)
Packing support	Cost of sieve trays(USD/m^2)× cross-sectional area of vessel
Distributor support	Cost of sieve trays(USD/m^2)× cross-sectional area of vessel
Distributor	(6/5) × Cost of distributor support
Scrubber packing	Weight of packing(kg) × cost of packing(USD/kg)
Reactor catalyst	Catalyst weight (kg) × cost of catalyst(USD/kg)

Costs of sieve trays, packing, and catalyst are 1123.5 USD/m^2, 8.79 USD/kg, and 150 USD/kg respectively [56].

4.2.8.2. OPEX

Annual operating costs are divided into two categories: fixed and variable. Fixed operating costs include labor and operations and maintenance (O&M) costs. Labor costs are considered to be 0.3% of TCI, and O&M costs to be 3% of TCI [54]. It should be noted that variable costs are estimated solely based on electricity costs. The cost of utilities, such as cooling water, are assumed to be insignificant in comparison to annual electricity costs. Renewable electricity costs are considered 0.0432 USD/kWh [57].

4.2.8.3. Cost estimation results and discussion

Total annualized cost is the sum of annual capital (CAPEX) and operating (OPEX) expenditures [54]. Annualized costs for a project lifetime of 20 years and an interest rate of 7% are compared for the three proposed designs. The findings of the estimations are shown in Figure 4.11. It is to be noted that these estimations follow the AACEI (Association for the Advancement Cost Engineering International) guidelines and are based on Class 5 estimations which are considered valuable for the feasibility analysis of a project [58].

The results demonstrate that design 2 provides the best economic performance. The implementation of this design would prevent 25.3 tons of hydrogen emissions annually. In Europe, carbon is currently taxed at 108 USD (or 100 EUR) per ton, which would result in an annual offset of about 0.1 Million USD, accounting for only 25% of the annual cost incurred for the most economical design. It implies that proposed solutions will continue to be costly. If such solutions are to be deployed in the future to prevent hydrogen emissions, hydrogen or CO_2 equivalents should be taxed at a higher rate than the current price to encourage the adoption of these designs. Furthermore, companies that adopt these designs should be given tax breaks or other incentives to encourage their use. Government should provide subsidies to aid in the implementation of such solutions. This will help to reduce the burden on businesses and consumers while also ensuring a smooth transition to a more sustainable green hydrogen-based economy.

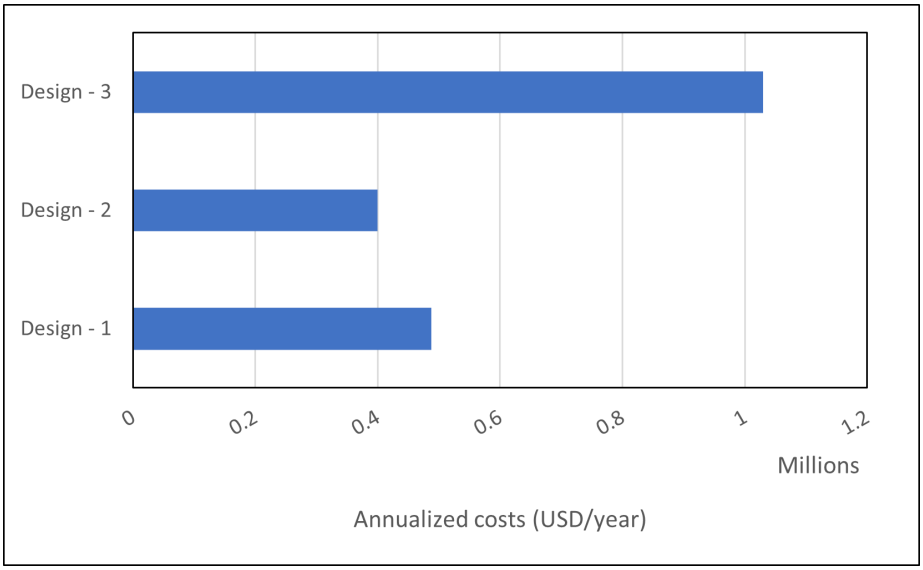

Figure 4.11: Economic analysis of different de-hydro designs

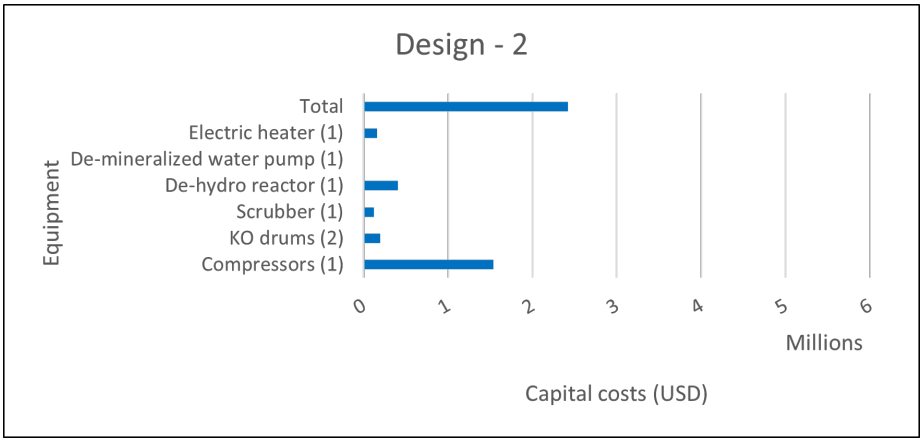

Figure 4.12: Capital costs breakdown

Figure 4.12 shows the breakdown of capital costs of design 2 by equipment. The findings show that the compressor cost is the largest contributor to the total capital costs of the design. However, it should be noted that a compressor is only required in the case of a low-pressure system; if the system pressure is high enough to withstand pressure drop in the scrubber and reactor, a compressor is not required. Furthermore, scrubbers are only required in alkaline systems. For example, a PEM system, as described in section 2.1, will not have KOH issues, so there will be no

need for scrubbing. Therefore, adding the de-hydro reactor to reduce emissions from hydrogen crossover could be viable for these cases.

4.3. Battery energy system (BES)

According to leakage assessments presented in chapter 3, the biggest contributor to the hydrogen emissions is venting due to frequent shutdowns and startups when the power is unavailable. Flaring the hydrogen released is determined as one of the feasible options to prevent hydrogen emissions. Another option could be to install a battery storage system to lessen the frequency of shutdowns. It even avoids burning the product and the risk of NOx emissions. Batteries can be used to store excess renewable energy and use it to supplement the minimal power needed to run the electrolyzers. This will prevent shorter-duration shutdowns and cut down on venting to the atmosphere. Firstly, different battery technologies are discussed. Then, the modeling of the battery energy system is described which is followed by a discussion of the results obtained and sensitivity analysis.

4.3.1. Different BES technologies

There is a wide range of various types of BES technologies based on different chemistries. Different battery technologies offer very unique battery performance characteristics in terms of charging and discharging efficiencies, lifetime, application suitability, and system costs. For instance, due to high self-discharge rates, battery technology suited for fast responses may not be ideal for long-term storage applications [59]. In this section, a few BES technologies that might be appropriate for stationary applications such as supplying the minimum load to the electrolysis unit are discussed.

1) Lithium-ion batteries: Lithium ions(Li^+) are exchanged between the anode and the cathode of Li-ion batteries, which are made from lithium intercalation compounds like lithium cobalt oxide($LiCoO_2$). Typically, graphite serves as the anode, and lithium metal oxide serves as the cathode [60]. Figure C.1 in the appendix C represents the general operating principle of these batteries.

Li-ion batteries have higher energy densities, excellent round-trip efficiencies, and longer lifetimes relative to other common battery storage technologies like lead-acid batteries [59]. However, when battery cathodes overheat, they can release oxygen and may lead to fires. This issue can cause thermal instability and safety concerns in Li-ion battery systems. In order to reduce safety concerns, consistent efforts are made to integrate effective thermal management and monitoring systems [61]. They are increasingly gaining dominance in stationary applications. Li-ion batteries can provide quite distinctive performance and cost characteristics based on various cathode materials [62], [63]. Three different types of Li-ion batteries are compared in this project. These three types are selected as they offer higher thermal stability compared to other possible combinations of lithium compounds [61], [64], [65].

Table 4.8 shows the key characteristics of these batteries. These are based on the anticipated projections for the year 2030.

Table 4.8: Characteristics of various types of Li-ion batteries [59], [66]–[68]

Key active material	**Lithium nickel cobalt aluminium (NCA)**	**Lithium iron phosphate (LFP)**	**Lithium nickel manganese cobalt oxide (NMC)**
Cathode	$LiNiCoAlO_2$	$LiFePO_4$	$LiNixMnyCo_{1-x-y}O_2$
Anode	C(graphite)	C(graphite)	C(graphite)
Calendar life (years)	18	18	18
Depth of discharge (%)	90	90	90
Round-trip efficiency (%)	97	94	97
Self-discharge (% per day)	0.2	0.1	0.1
Installation cost (USD/kWh)	145	224	167

2) Vanadium redox flow batteries: Flow batteries differ from conventional batteries as the electroactive materials are dissolved in the electrolyte solutions rather than stored in electrodes as in traditional batteries. The electrolyte solutions are stored separately in two separate tanks called the anolyte tank and catholyte tank. These tanks are separated from the cell stacks. Electrolytes are pumped into these regenerative cell stacks, where oxidation and reduction reactions take place [69]. The most mature redox flow battery technology is the vanadium redox flow battery system (VRFB). VRFB systems function on different oxidation states of vanadium and features V^{2+}/V^{3+} and V^{5+}/V^{4+} redox couples [70], [71]. Figure C.2 in the appendix C describes the working mechanism of a vanadium redox flow battery system.

In comparison to conventional rechargeable batteries, VRFB systems have a number of advantages, including the ability to operate at very close to ambient temperatures, longer lifespans, and lower costs due to the use of inexpensive raw materials involved. They are very well suited for large-scale stationary applications due to their higher thermal stability characteristics [72]. However, handling can be problematic because there is a chance that electrolyte solutions could leak. Another disadvantage is that they rely on moving components such as pumps, which can cause frequent breakdowns [73]. Despite their handling issues, VRFB systems have a lot of potential, and more advances are being made to prevent these issues [71].

3) Valve-regulated lead-acid batteries: Lead-acid batteries are the oldest and the most widely deployed battery systems. Pb-acid systems can be divided into two categories, flooded and valve-regulated batteries, based on two distinct design forms. Flooded lead-acid batteries are conventional lead-acid batteries, which consist of stacked cells immersed in the electrolyte solution of sulfuric acid. A porous membrane separates the lead metal anode (Pb) from the lead dioxide cathode (PbO_2) in each cell [61]. The fundamental workings of a lead-acid battery are illustrated in Figure C.3 in the appendix C.

Flooded lead-acid batteries are cheaper but pose safety concerns in providing large-scale services due to the gassing process during charging. When the cell voltage is higher than the water electrolysis voltage, which is roughly 2.4 volts, hydrogen and oxygen gassing can happen as a result of overcharging the battery. This effect also causes water loss in electrolyte which can cause permanent damage to the battery [70]. Valve-regulated lead-acid batteries also known as sealed batteries are an improvement to the gassing and water loss issues in the traditional flooded lead-acid batteries. The valve regulates the overpressure to prevent water loss in a way that the venting will only occur when the pressure exceeds 100 millibars in the cells. By maintaining internal pressure, the valve also aids in the recombination of hydrogen and oxygen. Compared to flooded lead-acid batteries, sealed lead-acid batteries are more expensive, but they provide better safety and longer lifetimes for large-scale applications [70], [74].

4) Sodium sulfur high-temperature batteries: Sodium sulfur (NaS) batteries contain solid ceramic electrolyte made of beta-aluminum and liquid active materials. To keep the active materials in a liquid state, these battery systems operate at high temperatures. Molten sodium is the most frequently used anode material, and molten sulfur is the most frequently used cathode material in sodium-sulfur batteries. Sodium ion transport across the ceramic electrolyte is responsible for storing and releasing energy [75], [76]. Figure C.4 in the appendix C describes the working mechanism of a NaS battery.

NaS battery systems offer high energy densities and low self-discharge rates relative to lead acid and vanadium redox flow batteries. They have a lot of potential due to longer lifespans and lower costs, but effective ion transport across the solid ceramic electrolyte is still a challenge [60], [69]. Additionally, it runs the risk of cross-contamination between molten sodium and sulfur and damaging ceramic electrolyte in the event of a crash [59], [77].
Table 4.9 presents the key performance characteristics of VRFB, sealed Pb-acid, and NaS battery technologies.

Table 4.9: Characteristics of VRFB, Pb-acid and NaS batteries [59]

Battery technologies	Vanadium redox flow (VRFB)	Sealed lead-acid	Sodium sulfur high-temperature
Cathode	V^{5+}/V^{4+}	PbO^2	Molten sulfur
Anode	V^{2+}/V^{3+}	Pb	Molten sodium
Calendar life (years)	19	13	24
Depth of discharge (%)	100	50	100
Round-trip efficiency (%)	78	83	85
Self-discharge (% per day)	0.15	0.25	0.05
Installation cost (USD/kWh)	119	132	162

4.3.2. Modeling of battery system

The aim of this model is to determine the optimum battery system capacity that may be installed in order to serve the minimum load when the available wind power is less than the minimum power needed by the electrolyzer system. The system's optimum capacity is the one with the lowest total cost, which includes the cost of the installed battery system and the cost associated with shutdowns. The cost of the battery system is assumed as simply the initial capital expenditure of the battery system. The capital cost of a battery system is calculated as the product of the installed capacity and the cost of the system per kWh installed [59]. Cost of shutdowns include:

1) Cost of nitrogen required for purging when the system is shutdown: The mass of nitrogen needed for purging is estimated based on the volume of the equipment that needs to be purged with nitrogen, the pressure that must be maintained in the system during the shutdown, and the pressure of the nitrogen header. For purging, normally five times the volume of the system is required. Cost of purging is obtained:

Mass of N_2 for purging = 5 Equipment volume * Pressure of system * Density of N_2/Pressure of N_2 header*
*Cost of purging = Mass of N_2 for purging * cost per kg of N_2*

2) Cost of venting hydrogen into the atmosphere: There are two instances in which hydrogen is released into the atmosphere, namely when it is still present in the system right after the system has been shut down and when it is released continuously following a start-up until the desired level of product purity has been reached. Based on operational experience, it's estimated to take two hours to achieve the

desired product specifications. The plant operates at 15% capacity during the first and second hours after startup. To penalize these hydrogen emissions, the CO_2 equivalents of the H_2 emissions are calculated as follows.

*Cost of H_2 emissions = Mass of H_2 vented * GWP of H_2 * Cost of CO_2 equivalent per ton*

3) Cost of the deferred hydrogen production: Hydrogen is vented for almost two hours after the unit has started up, and renewable power is available. Even though there is power during this time, the generated product is off specification and cannot be sold or used; this is termed deferred production.

*Cost of deferred production = (Available power/Maximum electrolyzer load) * Production at full load * Price of H_2 per kg*

If the battery system needs to be replaced during the project's lifespan, replacement costs are also included in the overall costs. The cost of the battery system's resale is also subtracted from the overall cost, assuming that the system can be sold at a discounted price if it has at least half of its lifetime left at the end of the project. These will be discussed in detail later in this section. All the calculations are based on the Present Value (PV) of costs incurred during the project lifetime.

The idea is that the battery system absorbs the peaks of the extra energy produced by renewable energy power plants and discharges when the power is not enough to support the minimum load to avoid a shutdown. In this manner, shorter-duration shutdowns can be avoided at an optimized capacity. The Hollandse Kust Noord (HKN) offshore wind power plant serves as the model for the wind profile (Appendix A). The data is scaled to an annual resolution of one hour and an average capacity of 100 MW. It is assumed that the wind power will remain constant for the entire hour and that the wind profile will be known beforehand.
The model is implemented in MATLAB and the control sequence of the model is captured in Figures 4.13, 4.14, and 4.15.

Every hour, it is checked if the amount of wind power is less than the minimum power required by the electrolyzer system. If this condition is true (figure:4.14), then the State of Charge (SoC) of the battery system is examined to determine whether it is greater than the minimum SoC. If so, the controller determines if the battery has enough energy to last the entire duration of the shutdown. If all of these conditions are met, the battery is discharged such that the available wind power and the power discharged from the battery together are sufficient to serve the minimum load of the electrolyzer. The cost of shutdowns is estimated based on whether the unit is in the first or second hour of operation. In that case, hydrogen is still released into the atmosphere, and the cost of hydrogen emissions must be considered. When a unit doesn't operate within the first or second hour of the startup, the system is incentivized by deducting the price of the hydrogen pro-

duced from the cost of the shutdowns. The electrolyzer system is shut down if any of these conditions are false and the battery system is charged with the available wind power. The cost of the shutdown in this case is estimated by determining whether it is a continued shutdown. If the shutdown is not continued, the electrolyzer system is nitrogen-purged, and the costs of N_2 purging and H_2 emissions are added. Otherwise, it is implied that the system has already been shut down and blanketed with nitrogen for at least the past one hour.

If wind power exceeds the electrolyzers' minimum and maximum power demands (figure:4.15), it is determined whether the unit is in its first or second hour of operation. In that situation, the unit is still venting while operating at minimum load i.e. 15% of its potential. Although there is sufficient wind power, the unit is still not operating at full capacity and the product is vented to the atmosphere because it does not meet specifications. Then the cost of shutdowns would be the price of deferred hydrogen production and the cost of H_2 emissions. Then, the SoC of the battery system is checked, and if it is less than the maximum SoC, batteries are charged using power in excess of the minimum electrolyzer load. In the alternate scenario, where the unit is not in the first or second hour, the unit is operating at full capacity and the battery system's SoC is examined; if it is less than the maximum SoC, the batteries are charged using the excess power. If not, it is assumed that extra power will be discharged outside the system. There are no shutdown costs in this situation.

In another case, when the wind power is greater than the minimum electrolyzer load but less than the maximum electrolyzer load (figure:4.15), and if the unit is in the first/second hour after starting up, the SoC is checked. Batteries are charged if the SoC is less than the maximum SoC. Costs associated with shutdowns include the price of deferred hydrogen production and the cost of hydrogen emissions during venting. When the unit is not in its first or second hour of the startup, the system is operating at the wind power available and there are no shutdown costs.

The final scenario is when there is just enough wind power to supply the minimal electrolyzer load (figure:4.15). In this case, the model determines whether the unit is within the first or second hour of the startup, and if it is, the cost of the shutdown would be equal to the sum of the price of deferred production and the cost of hydrogen emissions. Otherwise, the system is operating at minimum electrolyzer load and generating hydrogen product with no costs associated.
It should be noted that when the battery system is charged or discharged, the SoC of the system is maintained between the minimum and maximum SoC at all times. The model checks these conditions every hour of the year and calculates the annual cost of shutdowns for each capacity (figure:4.13). The present value of the cost of shutdowns over the project lifetime is evaluated as:

$$PV(\text{Cost of shutdowns}) = \Sigma \text{Cost of shutdowns over an year} * (1+inflation)^n / (1+r)^n$$

n ranges from 0 to project lifetime and r is the rate of interest.

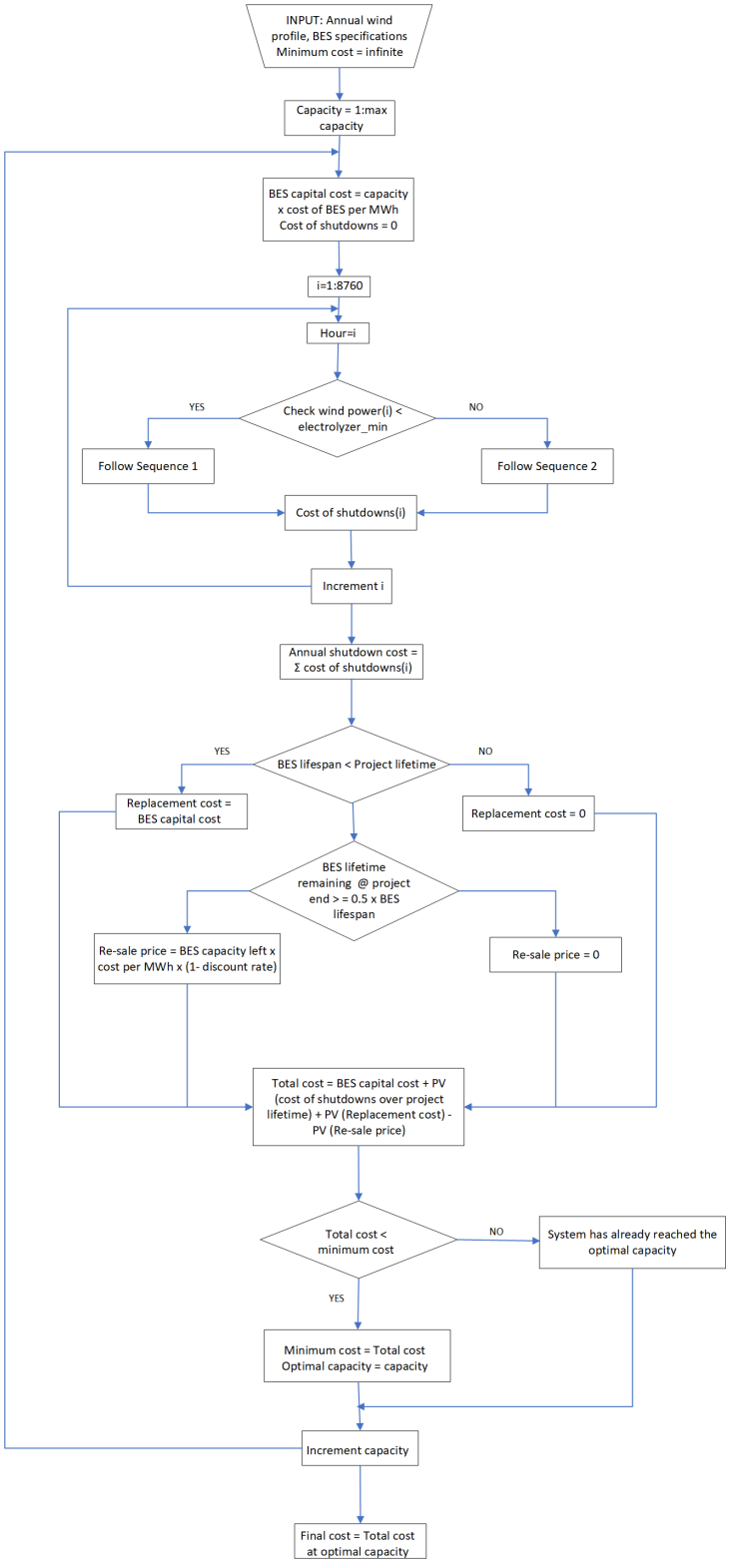

Figure 4.13: Battery Energy System(BES) - Controller modelling flow

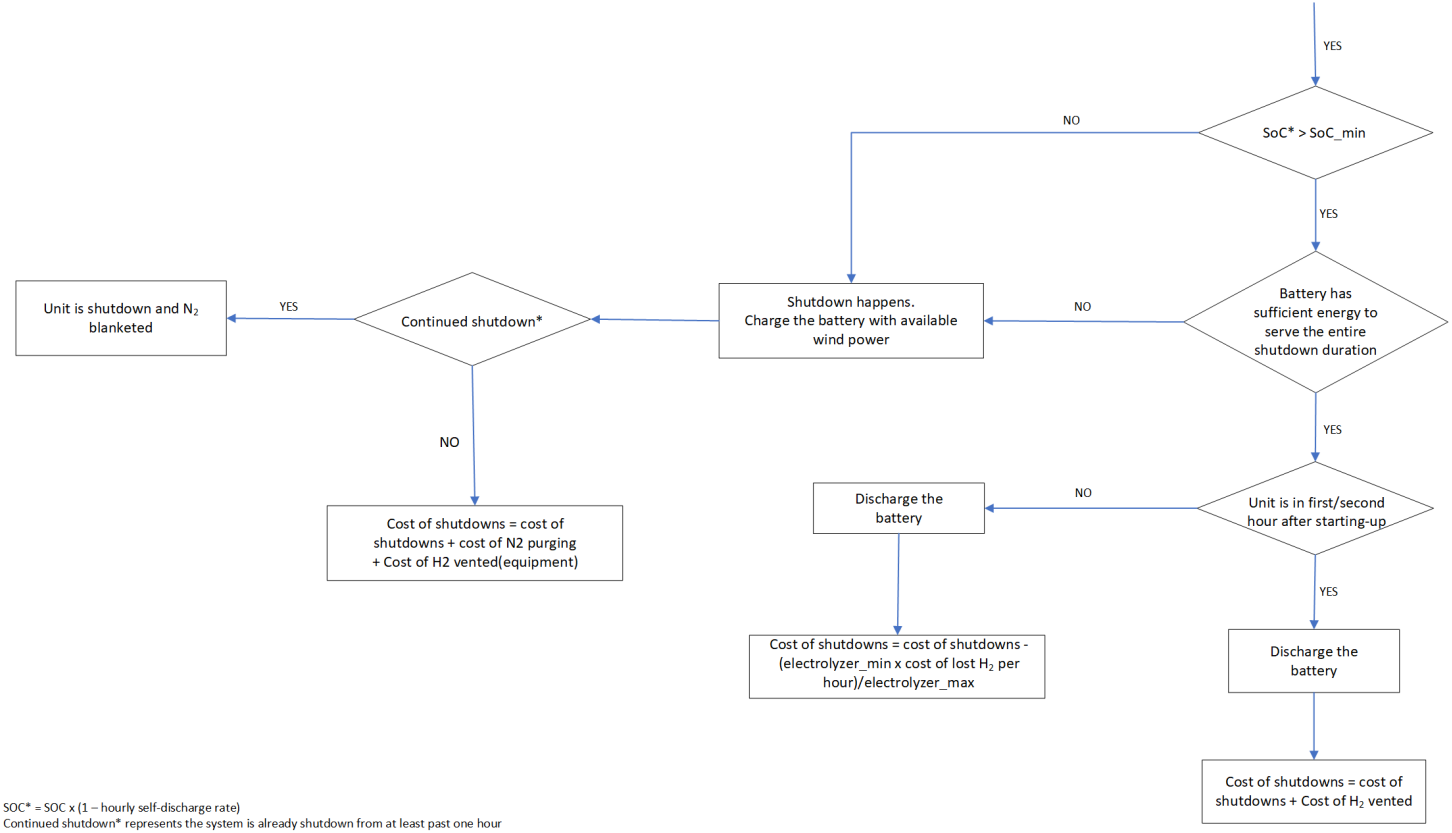

Figure 4.14: Battery Energy System(BES) - Flow sequence 1

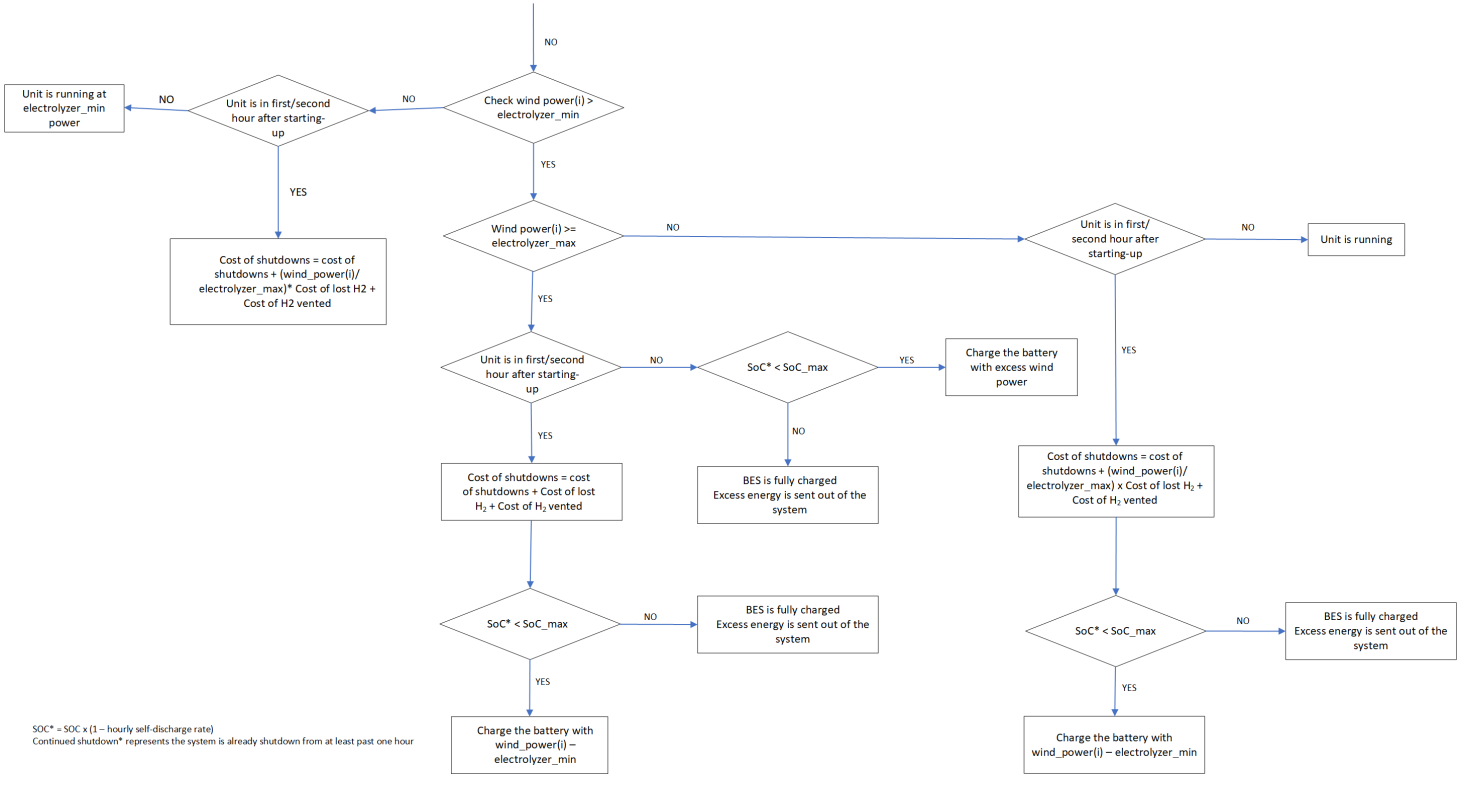

Figure 4.15: Battery Energy System(BES) - Flow sequence 2

Whether or not the battery system needs to be replaced depends on its lifetime. When the battery system's lifespan is less than the project's lifespan, replacement is needed and the costs, which are estimated using the given relation, are added to the overall costs. This calculation assumes that the cost of the battery system remains constant during the beginning of the project as well as when the replacement is needed.

PV(Replacement cost) = Capital cost of the battery system/$(1+r)^{BES-lifetime}$

The re-sale of the battery system is taken into account only if the battery system has half or more years of life left at the end of the project. In order to determine whether the system qualifies for re-sale, the model checks if the replacement cost is positive and the project lifetime is less than or equal to 1.5 times the lifetime of the battery system. If both conditions are true, the system is deemed resellable, and the re-sale price is evaluated from the given relation. The system would presumably be sold at a set discount rate at the end of the project.

*PV(Re-sale price) = Capital cost of the battery system * (1-discount rate) * (2*BES lifetime - Project lifetime)/(BES lifetime)/*$(1+r)^{Project-lifetime}$

If the aforementioned condition is false, the model determines if the battery system lifetime is at least twice as long as the project lifetime, in that case, the re-sale price's present value is:

*PV(Re-sale price) = Capital cost of the battery system * (1-discount rate) * (BES lifetime - Project lifetime)/(BES lifetime)/*$(1+r)^{Project-lifetime}$

Then the net present value of the total cost of the system is estimated as:
NPV(Total costs) = Capital cost of the system + PV(Cost of shutdowns) + PV(Replacement cost) - PV(Re-sale price)

Total costs for each capacity are calculated and the one with the lowest total cost is reported as the optimum capacity.

4.3.3. Model Inputs and Results

This section presents and discusses the outcomes of the base case technology. Vanadium flow redox battery technology is chosen as the base case because it offers very low installation costs relative to other batteries like Li-ion and NaS battery technologies. As indicated in the section 4.3.1, VRFB batteries provide higher thermal stability and longer lifetimes, therefore are very well suited for large-scale stationary applications. In order to estimate the optimum capacity, several of the model's inputs, including the minimum and maximum State of Charge(SoC), charging and discharging efficiency, battery system lifetime, cost per MWh, and daily self-discharge rate are technology-specific to particular battery types and are listed in the table 4.10. These are based on the projections for 2030 [59] when most

battery technologies are anticipated to have reached their peak of development. The table 4.11 provides additional inputs to the model, such as the minimum and maximum electrolyzer power load, project lifetime, cost of N_2 and H_2 etc.

Table 4.10: Battery technology specific model inputs

Battery-specific characteristics	Model inputs
Minimum SoC (%)	10
Maximum SoC (%)	90
Battery system lifetime (years)	19
Charging efficiency(%)	88
Discharging efficiency (%)	88
Self-discharge (% per day)	0.15
Installation cost (USD/kWh)	119

Table 4.11: Other input parameters

Parameters	Model inputs
Minimum electrolyzer load (MW)	15
Maximum electrolyzer load (MW)	100
Project lifetime (years)	20
Interest rate, r (%)	7
Discount rate (%)	10
Inflation (%)	2
Maximum capacity (MWh)	1000
Cost of N_2 (USD/ton)	129.6
Cost of CO_2 equivalents (USD/ton)	108
Price of green H_2 (USD/ton) [78]	11500
GWP of H_2	33
Density of N_2 (kg/m^3)	15.57
Pressure of N_2 header (kPa)	1300
System pressure (kPa)	105

The trend of the system costs with the increasing capacity of the vanadium redox flow battery system is depicted in Figure 4.16. As installed capacity increases, the number of shutdowns reduce and shutdown costs go down and the battery system costs rise as expected. Up until a certain point, as shutdown costs decrease, so do system total costs. After a certain point, a decrease in shutdown costs is no longer enough to offset the increase in the price of the battery system, resulting in

an upward trend in overall costs. The vanadium redox flow battery systems reach their peak performance at 158 MWh and a total project cost of -1.69 million USD. The negative sign indicates that the battery system generates more revenue and reduces costs by preventing shutdowns than the capital invested in it. The number of shutdowns estimated before and after the installation of the battery system are 152 and 84 every year, respectively. Also, installation of BES leads to a 46% decrease in H_2 emissions over the course of a year. Installing higher capacities than the optimal capacity can cut emissions by a greater amount, but doing so will result in overall costs that are higher than the minimum value. As evident from the section 4.3.2, it is crucial to keep in mind that the entire cost is dependent on a number of factors, including the price of nitrogen, the tax on H_2 emissions, the price of hydrogen product, and the initial investment in battery systems. The optimal capacity and the overall costs involved may change if any of these characteristics are changed. The section 4.3.4 analyzes the sensitivity of the model outputs when any of these factors are altered.

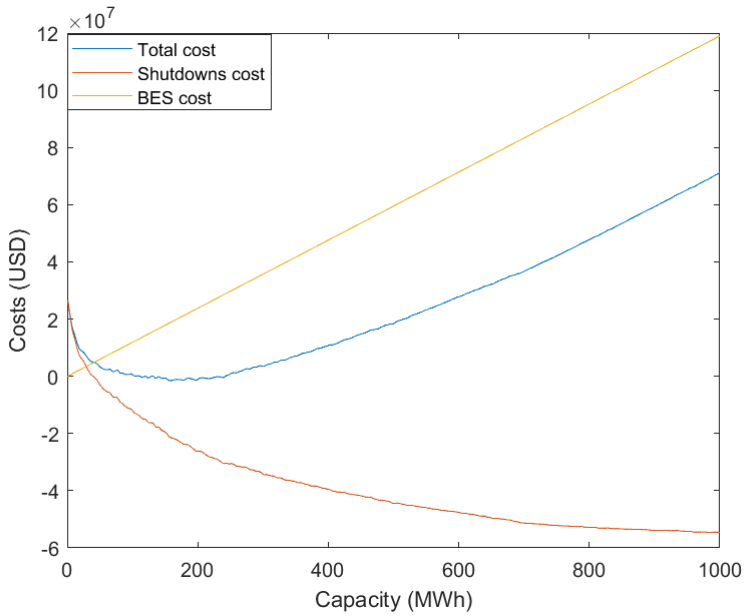

Figure 4.16: Cost vs capacity in vanadium redox flow battery system

4.3.4. Sensitivity Analysis

For the model to be used in the future, it is essential to comprehend how various parameters affect the model outputs. Even if the battery system has already reached the top of the learning curve, factors like utility costs, and hydrogen taxes are bound to change. Sensitivity analysis aids in more accurate outcome prediction based on a set of parameters. It also provides insight into how sensitive the best

solution is to changes in the input variables' values. The sensitivity to the specific input variable is calculated by dividing the percent change in the output over the percent change in the input parameter. To do a sensitivity study, the following parameters are changed by +/-50% from their base value.
1) Cost of N_2 required for purging
2) Cost of CO_2 equivalents of hydrogen emissions
3) Price of green H_2
4) Capital cost of battery system

Tables 4.12, 4.13, 4.14 and 4.15 list the findings of the sensitivity analysis. Normalized cost is estimated by dividing the total cost obtained at optimized capacity by optimal capacity. The results clearly show that the normalized cost is highly sensitive to changes in the price of green hydrogen and the capital costs of battery systems. It should also be noted that an increase in the value of each parameter results in higher costs, with the price of hydrogen being the exception. These findings are consistent with the fact that shutdown costs climb when N_2 purging and H_2 emissions costs rise, which raises overall costs. However, the system exhibits little sensitivity to variations in the price of hydrogen emissions and nitrogen purging. Only the costs at which the optimal capacity is reached change; the optimal capacity remains constant. This implies that these costs aren't high enough that even varying them doesn't significantly change the shutdown costs, which could change the optimal capacity. BES costs have a direct impact on the investment required to install the battery system; thus, higher BES costs lead to lower optimal capacities and higher normalized costs. According to Table 4.14, the overall cost decreases as the price of green hydrogen rises. A higher price for green hydrogen would mean larger incentives in generating hydrogen when shutdown is avoided by BES, but it would also mean bigger losses in the form of deferred hydrogen production expenses. The sensitivity results show that the incentive from fewer shutdowns overcomes the loss from higher deferred production costs, with the outcome being a reduction in overall costs.

Table 4.12: Sensitivity by varying N_2 cost

Input parameter	**Cost of Nitrogen**		
% change	**- 50%**	**Base Case**	**+ 50%**
Input cost of nitrogen (USD/ton)	64.8	129.6	194.4
Optimum capacity (MWh)	158 MWh	158 MWh	158 MWh
Total cost at optimized capacity (Million USD)	-1.79	-1.69	-1.59
Normalized cost (Million USD/MWh)	-0.0113	-0.0107	-0.0101
% change in normalized cost	- 6.1%	Base Case	+ 6.1%
Sensitivity to normalized cost	+ 12.1%	Base Case	+ 12.1%

Table 4.13: Sensitivity by varying CO_2 eqv cost

Input parameter	**Cost of CO_2 equivalents**		
% change	**- 50%**	**Base Case**	**+ 50%**
Input cost of CO_2 eqv (USD/ton)	54	108	162
Optimum capacity (MWh)	158 MWh	158 MWh	158 MWh
Total cost at optimized capacity (Million USD)	-2.77	-1.69	-0.61
Normalized cost (Million USD/MWh)	-0.0175	-0.0107	-0.0038
% change in normalized cost	-64.1%	Base Case	+64.1%
Sensitivity to normalized cost	+ 128.1%	Base Case	+ 128.1%

Table 4.14: Sensitivity by varying green H_2 price

Input parameter	**Price of green H_2**		
% change	**- 50%**	**Base Case**	**+ 50%**
Input price of green H_2 (USD/kg)	5.75	11.5	17.25
Optimum capacity (MWh)	37	158	238
Total cost at optimized capacity (Million USD)	6.29	-1.69	-16.6
Normalized cost (Million USD/MWh)	0.17	-0.0107	-0.07
% change in normalized cost	+1687.6%	Base Case	-552.5%
Sensitivity to normalized cost	-3375%	Base Case	-1105%

Table 4.15: Sensitivity by varying BES capital cost

Input parameter	**BES capital cost**		
% change	**- 50%**	**Base Case**	**+ 50%**
Costs of BES (USD/kWh)	59.5	119	178.5
Optimum capacity (MWh)	301	158	69
Total cost at optimized capacity (Million USD)	-15.6	-1.69	5.73
Normalized cost (Million USD/MWh)	-0.052	-0.0107	+0.083
% change in normalized cost	-384.2%	Base Case	+875.8%
Sensitivity to normalized cost	+768.4%	Base Case	+1751.6%

4.3.5. Comparison of different BES technologies

The section 4.3.1 discusses various battery technologies and their characteristics. This section compares these technologies based on the model's findings. All of these technologies are distinct in terms of charging and discharging efficiencies, system lifetimes, self-discharge rates, installation costs, and so on. These inputs are provided to the model for each technology based on the parameters listed in tables 4.8 and 4.9. Other non-battery technology-specific parameters described in table 4.11 remain unchanged. The comparison is done on the basis of the optimum capacity obtained as well as the normalized cost for each technology. The obtained results are recorded in the table 4.16.

Table 4.16: Comparison of different battery technologies

Battery technologies	Optimum capacity (MWh)	Total cost at optimized capacity (Million USD)	Normalized cost (Million USD/MWh)
Vanadium redox flow	158	-1.69	-0.0107
Li-ion NCA	138	0.51	0.0037
Li-ion NMC	97	3.02	0.0311
NaS high-temperature	82	2.67	0.0326
Li-ion LFP	49	7.34	0.1498
Sealed lead-acid	56	10.84	0.193

Vanadium redox flow battery systems are the only ones that offset more expenses than invested over the course of the project, as is clear from the findings provided in Table 4.16. It could be due to their low installation costs because sensitivity analysis in the section 4.3.4 shows that the system is highly sensitive to the BES costs. The Li-ion NCA system, which has a high-efficiency round-trip and low price, is the second-best technology. It is also important to note that systems with higher optimal capacities would be more advantageous because larger installed capacities can prevent a greater number of shutdowns.

Intermittency is becoming an inevitable part of the energy system as the percentage of renewable technologies in the energy sector rises, leading to more frequent shutdowns due to power shortages. Battery systems are the most cost-effective way to reduce the number of shutdowns and thus limit hydrogen emissions in the future green hydrogen economy. According to the various analyses presented in the sections 4.11, 4.3.4 and 4.16, installing battery energy systems as a way to lessen the frequency of shutdowns in a fully green hydrogen production unit is feasible and merits further investigation.

Power purchase agreements (PPAs) could be another temporary solution to battery systems. A power purchase agreement is a long-term power contract between two parties, one of which is a power producer. Green Power Purchase Agreements

(Green PPAs) are becoming increasingly popular, with companies purchasing these contracts gaining access to certified green power at a stable, reliable, and predefined rate [79]. This ensures that electrolyzer systems are always supplied with the minimum load required. However, when the major share of power is generated from renewable sources, intermittency is unavoidable. As a result, Green PPAs can only act as short-term substitutes for battery systems.

4.4. Conclusions

This chapter discusses the potential solutions to hydrogen emissions. The major contributions from this chapter are listed below:

1. Flaring system: It is mentioned as one of the solutions to the emissions due to frequent shutdowns and startups. Vented hydrogen can be combusted at the tip of the flare system. However, hydrogen combustion is conducive to NOx formation due to its high adiabatic flame temperatures. Therefore, NOx emissions from hydrogen flaring are investigated to determine the feasibility of this solution. The NOx formation from a 100 MW green hydrogen unit is approximately 2% of the NOx formation from the same capacity of a grey hydrogen plant. Flaring is considered a feasible option but only temporarily, until other permanent solutions, such as battery systems, can be implemented.

2. De-hydro reactor: Catalytic recombination of hydrogen and oxygen is investigated to prevent hydrogen emissions from hydrogen crossover in the electrolyzer. A reactor is modeled and optimized using the MATLAB program to predict the behavior of the de-hydro reactor. The obtained model is validated using the vendor data for the de-oxidizer reactor. The catalyst, 0.5 wt% Palladium on special alumina, is extremely sensitive to the electrolyte KOH used in the alkaline electrolysis unit. To prevent catalyst poisoning by KOH, the following three designs are proposed which could be implemented to reduce hydrogen emissions:

    - Design 1: Single-stage compression followed by scrubber and de-hydro reactor.
    - Design 2: Single-stage compression followed by scrubber, heater, and de-hydro reactor.
    - Design 3: Three stages of compression followed by the de-hydro reactor.

    All proposed designs are simulated in UNISIM, and each equipment is sized to determine the economic viability of the designs. The annualized cost of each design is calculated by estimating capital and operational expenditures. Design 2 is found to be the most economical design with an annualized cost of 0.4 Million USD, however, the annual cost offset by implementing this design is 0.1 Million USD only. In order to prevent crossover emissions in low-pressure alkaline systems, it is determined that implementing this solution is not economically feasible and necessitates government incentives. This chapter also emphasizes that such designs are case-specific and that adding a de-hydro

reactor can become more cost-effective in other situations. For example, high-pressure PEM electrolysis does not require a scrubber because no alkaline electrolyte is present, nor does it require a compressor system because the pressure is sufficient to handle the pressure drop in the de-hydro reactor. This could significantly reduce the cost of the systems, but because this study is based on low-pressure alkaline, it is not investigated.

3. Battery Energy System(BES): Battery systems can avoid frequent shutdowns and startups, reducing the amount of hydrogen venting. In comparison to combusting the hydrogen product, they are a more long-term solution. The various battery storage technologies suitable for stationary applications, such as supplying a minimum load to the electrolyzers, are discussed. The MATLAB model used to determine the optimized capacity of the battery system is described in detail in this chapter. When the total costs, which primarily include the cost of the system and the cost of shutdowns, are at their lowest, the optimum capacity is reached. The modeling results for vanadium flow redox battery (VRFB) systems show that these systems generate more revenue than the battery system's capital investment over the project's lifetime. The sensitivity analysis is performed to better understand the model's behavior, and it reveals that changes in hydrogen prices and battery system installation costs have the greatest impact on overall system costs. Different battery technologies are also compared in terms of total costs and capacities, revealing that VRFB systems provide the maximum incentive and largest optimal capacities when compared to other technologies. The findings of the study back up the feasibility of battery energy systems for reducing hydrogen emissions.

5

Conclusions

Green hydrogen produced from renewable sources is expected to be critical in the energy transition. However, evidence suggests that hydrogen has the potential to be an indirect greenhouse gas with a GWP as high as 33 in comparison to carbon dioxide. When hydrogen leaks into the atmosphere, it reacts with hydroxyl radicals to form water. These hydroxyl radicals would otherwise neutralize the greenhouse gases like methane in the atmosphere. Therefore, hydrogen indirectly increases the lifespan of methane, thereby classifying it as an indirect greenhouse gas. In this thesis project, emissions in a green hydrogen electrolysis unit are estimated and analyzed, and a feasibility analysis of potential solutions is conducted.

Based on the current literature, Chapter 2 provides an overview of the basic principles of various electrolysis technologies, discusses the sources of leakages in the electrolysis unit, and includes a discussion of the global warming potential of hydrogen.

The primary assumptions which form the basis of leakage estimations are discussed in chapter 3. The adapted estimation methodology and results obtained are also discussed in detail. The results highlight that it is worthwhile to switch from grey to green hydrogen, but that green hydrogen emissions also need to be kept under control in order to achieve net zero emissions in the future.

Chapter 4 discusses the potential solutions to hydrogen emissions. The major contributions from this chapter are listed below:

1. Flaring system: Flaring is deemed a viable option, but only temporarily, until other permanent solutions, such as battery energy systems, can be implemented.

2. De-hydro reactor: A reactor to catalytically recombine hydrogen and oxygen is modeled in MATLAB. In order to reduce emissions caused by hydrogen cross-over in the electrolyzer, the economic viability of a few designs suitable

for a low-pressure alkaline electrolysis system is discussed. The most cost-efficient design is the one with the single-stage compression, then a scrubber to remove KOH, an electric heater, and a de-hydro reactor to finally remove the hydrogen present. However, the cost offset by reducing hydrogen emissions is only 25% of the annualized cost of the design. It is concluded that implementing this solution to prevent emissions due to crossover is not cost-efficient and requires incentives from the government.

3. Battery Energy System(BES): Installing battery systems to reduce the frequency of shutdowns and startups, as well as hydrogen emissions, is a more long-term solution than flaring the hydrogen product. This section describes in detail the MATLAB model used to determine the optimized capacity of the battery system. The modeling results for vanadium flow redox battery (VRFB) systems show that these systems generate more revenue throughout the project than the capital investment required for the battery system. The findings of this study support the viability of battery energy systems to reduce hydrogen emissions.

6

Recommendations

The leakage calculations in chapter 3 are based on the assumption that all green hydrogen production is done via low-pressure alkaline electrolysis. It should be noted that the amount of hydrogen emitted may vary depending on the production technology. However, these projections are sufficient to grasp the depth of the emerging issue of hydrogen emissions. Although, it is recommended that leakage sources be investigated on a case-by-case basis to determine the need for solutions. Moreover, fugitive emissions from flanges, valves, and seals are estimated based on the emissions factors available for methane leaks and are corrected to obtain values for hydrogen leaks. This is done due to the unavailability of monitoring data and emission factors for hydrogen leaks. When hydrogen leakage data is available, it is advised that the obtained results be validated.

Chapter 4 examines the technical and economic viability of three potential solutions for reducing hydrogen emissions from a green hydrogen plant. There are a few suggestions for the proposed solutions that could be considered:

1. De-hydro reactor: To prevent crossed-over hydrogen from entering the atmosphere, a reactor for catalytic recombination of hydrogen and oxygen is modeled. By assuming plug flow and a one-dimensional heterogeneous model, the reactor modeling is simplified. Validation of the reactor model demonstrates that these simplifications are adequate for determining the solution's feasibility. However, the level of detail in the model can be significantly improved in order to obtain a more realistic representation of the reactor for industrial implementation. It could be expanded to include a two-dimensional model. Furthermore, due to a lack of information about the porous structure of the catalyst, the catalyst effectiveness factor is assumed to be a constant value obtained from the literature. In reality, it may vary depending on the temperature. As a result, if the catalyst pore radius is known, the model can be improved to get a more accurate prediction of the catalyst effectiveness factor.

Following the modeling of the reactor, three designs for a low-pressure alkaline system are proposed. The compressor is required due to the low-pressure system, and the catalyst of the de-hydro reactor is highly sensitive to KOH, so the scrubber is also required. The least expensive design for a low-pressure alkaline system is still cost-inefficient in terms of the costs it offsets over the project's lifetime. However, if the de-hydro reactor is used for PEM, the scrubber is not required, nor is the compressor in the case of any high-pressure system. The compressor's capital cost is the most significant contributor to total system costs. As a result, it is recommended that the economic viability of the de-hydro reactor be determined on a case-by-case basis in order to make an informed decision.

2. Battery energy system (BES): The battery energy system is modeled in order to determine the optimal capacity that must be installed to reduce the shorter duration shutdowns. The model only takes into account the initial capital expenditure as the cost of the battery system. However, battery systems, particularly VRFB systems with moving components such as pumps, can have significant operational and maintenance costs. The model can be improved further by including the system's operational and maintenance costs. The model could also account for battery system degradation.

Bibliography

[1] 'Fugitive Hydrogen Emissions in a Future Hydrogen Economy,' Frazer-Nash Consultancy, Tech. Rep., 2022. [Online]. Available: www.gov.uk/government/publications/fugitive-hydrogen-emissions-in-a-future-hydrogen-economy.

[2] IPCC, 'Global Warming of 1.5°C,' Tech. Rep., Jun. 2018. DOI: https://doi.org/10.1017/9781009157940.

[3] IRENA, 'Green hydrogen: A guide to policy making,' Tech. Rep., 2020. [Online]. Available: www.irena.org/publications.

[4] DNV, 'Hydrogen forecast to 2050,' Tech. Rep., 2022. [Online]. Available: https://www.dnv.com/focus-areas/hydrogen/forecast-to-2050.html.

[5] N. Warwick, P. Griffiths, J. Keeble, A. Archibald and J. Pyle, 'Atmospheric implications of increased Hydrogen use,' Tech. Rep., 2022. [Online]. Available: https://www.gov.uk/government/publications/atmospheric-implications-of-increased-hydrogen-use.

[6] IRENA, 'GREEN HYDROGEN COST REDUCTION,' The International Renewable Energy Agency, Tech. Rep., 2020. [Online]. Available: http://www.irena.org/publications.

[7] A. Ursua, L. M. Gandia and P. Sanchis, 'Hydrogen Production From Water Electrolysis: Current Status and Future Trends,' *Proceedings of the IEEE*, 2012.

[8] A. Kovač, D. Marciuš and L. Budin, 'Solar hydrogen production via alkaline water electrolysis,' *International Journal of Hydrogen Energy*, Apr. 2019.

[9] S. A. Grigoriev, V. N. Fateev, D. G. Bessarabov and P. Millet, 'Current status, research trends, and challenges in water electrolysis science and technology,' *International Journal of Hydrogen Energy*, Oct. 2020.

[10] S. Sebbahi, N. Nabil, A. Alaoui-Belghiti, S. Laasri, S. Rachidi and A. Hajjaji, 'Assessment of the three most developed water electrolysis technologies: Alkaline Water Electrolysis, Proton Exchange Membrane and Solid-Oxide Electrolysis,' *Materials Today: Proceedings*, Jan. 2022.

[11] J. Chi and H. Yu, 'Water electrolysis based on renewable energy for hydrogen production,' *Chinese Journal of Catalysis*, Mar. 2018.

[12] P. D. Cavaliere, A. Perrone and A. Silvello, 'Water Electrolysis for the Production of Hydrogen to Be Employed in the Ironmaking and Steelmaking Industry,' *Metals*, 2021.

[13] A. Buttler and H. Spliethoff, 'Current status of water electrolysis for energy storage, grid balancing and sector coupling via power-to-gas and power-to-liquids: A review,' *Renewable and Sustainable Energy Reviews*, Feb. 2018.

[14] Y. Leng, G. Chen, A. J. Mendoza, T. B. Tighe, M. A. Hickner and C.-Y. Wang, 'Solid-State Water Electrolysis with an Alkaline Membrane,' *Journal of the American Chemical Society*, 2012.

[15] I. Vincent and D. Bessarabov, 'Low cost hydrogen production by anion exchange membrane electrolysis: A review,' *Renewable and Sustainable Energy Reviews*, Jan. 2018.

[16] G. Merle, M. Wessling and K. Nijmeijer, 'Anion exchange membranes for alkaline fuel cells: A review,' *Journal of Membrane Science*, Jul. 2011.

[17] IEA, 'The Future of Hydrogen,' Tech. Rep., 2019. [Online]. Available: https://www.iea.org/reports/the-future-of-hydrogen.

[18] M. Ozturk and I. Dincer, 'A comprehensive review on power-to-gas with hydrogen options for cleaner applications,' *International Journal of Hydrogen Energy*, Sep. 2021.

[19] G. R. Astbury, 'Venting of low pressure hydrogen gas a critique of the literature,' *Process Safety and Environmental Protection*, 2007.

[20] I. B. Ocko and S. P. Hamburg, 'Climate consequences of hydrogen emissions,' *Atmospheric Chemistry and Physics*, Jul. 2022.

[21] A. Arrigoni and L. Bravo Diaz, 'Hydrogen emissions from a hydrogen economy and their potential global warming impact,' Publications Office of the European Union, Luxembourg, Tech. Rep., 2022. [Online]. Available: https://publications.jrc.ec.europa.eu/repository/handle/JRC130362.

[22] National Oceanic and Atmospheric Administration(NOAA), *Climate Forcing*. [Online]. Available: Climate.gov.

[23] F. Paulot, D. Paynter, V. Naik, S. Malyshev, R. Menzel and L. W. Horowitz, 'Global modeling of hydrogen using gfdl-am4. 1: Sensitivity of soil removal and radiative forcing,' *International Journal of Hydrogen Energy*, 2021.

[24] R. G. Derwent, D. S. Stevenson, S. R. Utembe, M. E. Jenkin, A. H. Khan and D. E. Shallcross, 'Global modelling studies of hydrogen and its isotopomers using STOCHEM-CRI: Likely radiative forcing consequences of a future hydrogen economy,' *International Journal of Hydrogen Energy*, 2020.

[25] R. W. Howarth and M. Z. Jacobson, 'How green is blue hydrogen?' *Energy Science & Engineering*, 2021.

[26] U.S. Energy Information Administration, *Carbon Dioxide Emissions Coefficients*, 2022. [Online]. Available: https://www.eia.gov/environment/emissions/co2_vol_mass.php.

[27] A. T-Raissi and D. Block, 'Hydrogen: automotive fuel of the future,' *IEEE Power and Energy Magazine*, 2004.

[28] R. W. Howarth, 'A bridge to nowhere: methane emissions and the greenhouse gas footprint of natural gas,' *Energy Science & Engineering*, 2014.

[29] T. Smolinka, E. T. Ojong and J. Garche, 'Hydrogen Production from Renewable Energies—Electrolyzer Technologies,' *Electrochemical Energy Storage for Renewable Sources and Grid Balancing*, Jan. 2015.

[30] T. M. Shires, C. J. Loughran, S. Jones and E. Hopkins, 'Compendium of Greenhouse Gas Emissions Estimation Methodologies for the Oil and Natural Gas Industry,' Tech. Rep., 2009. [Online]. Available: https://ww2.arb.ca.gov/sites/default/files/2020-04/API%20Compendium%202009.pdf.

[31] H. Mathurkar, 'Minimum ignition energy and ignition probability for Methane, Hydrogen and their mixtures,' Ph.D. dissertation, 2015. [Online]. Available: https://hdl.handle.net/2134/19907.

[32] Ian Tiseo, *Annual carbon dioxide emissions in Denmark from 1970 to 2021*, 2023. [Online]. Available: https://www.statista.com/statistics/449517/co2-emissions-denmark/#:~:text=Denmark%20produced%2028.1%20million%20metric,caused%20dramatic%20emission%20reductions%20worldwide..

[33] N. C. Susanna Twidale Kate Abnett, 'EU carbon hits 100 euros taking cost of polluting to record high,' *Reuters*, 2023. [Online]. Available: https://www.reuters.com/markets/carbon/europes-carbon-price-hits-record-high-100-euros-2023-02-21/.

[34] J. Guarco, B. Langstine and M. Turner, 'Practical Considerations for Firing Hydrogen Versus Natural Gas,' *Combustion Engineering Association*, [Online]. Available: https://cea.org.uk/practical-considerations-for-firing-hydrogen-versus-natural-gas/.

[35] Queensland Government, *Nitrogen oxides*, 2022. [Online]. Available: https://www.qld.gov.au/environment/management/monitoring/air/air-pollution/pollutants/nitrogen-oxides#:~:text=Environmental%20and%20health%20effects%20of%20nitrogen%20oxides&text=High%20levels%20of%20nitrogen%20dioxide%20are%20also%20harmful%20to%20vegetation,visibility%2C%20and%20react%20with%20surface.

[36] U.S. Environmental Protection Agency (EPA), 'AP-42 Emissions Factors Chapter 13: Miscellaneous Sources,' Tech. Rep., 2019. [Online]. Available: https://www.epa.gov/air-emissions-factors-and-quantification/ap-42-fifth-edition-volume-i-chapter-13-miscellaneous-0.

[37] V. M. Torres, S. Herndon, E. Wood, F. M. Al-Fadhli and D. T. Allen, 'Emissions of nitrogen oxides from flares operating at low flow conditions,' *Industrial and Engineering Chemistry Research*, Oct. 2012.

[38] A. Frassoldati, T. Faravelli and E. Ranzi, 'A wide range modeling study of NOx formation and nitrogen chemistry in hydrogen combustion,' *International Journal of Hydrogen Energy*, Dec. 2006.

[39] R. H. Perry and D. W. Green, *Perry's Chemical Engineers' Handbook*. [Online]. Available: https://www.academia.edu/25001922/Perrys_Chemical_Engineer_Handbook_7th_Edition.

[40] LFG Technologies, *Low NOx Enclosed Flares*. [Online]. Available: http://lfgtech.com/portfolio-view/low-nox-enclosed-flares/.

[41] K. C. Sandeep, R. Bhattacharyya, C. Warghat, K. Bhanja and S. Mohan, 'Experimental investigation on the kinetics of catalytic recombination of hydrogen with oxygen in air,' *International Journal of Hydrogen Energy*, Oct. 2014.

[42] A. A. Iordanidis, *Mathematical modeling of catalytic fixed bed reactors*. Twente University Press, 2002. [Online]. Available: https://core.ac.uk/download/pdf/11456961.pdf.

[43] Scott Fogler H, *Elements of chemical reaction engineering*, 4th. Prentice Hall of India Pvt Ltd., 2006.

[44] API, 'API Standard 618 - Reciprocating Compressors for Petroleum, Chemical, and Gas Industry Services,' Tech. Rep., 2011. [Online]. Available: https://mycommittees.api.org/standards/techinterp/refequip/Shared%20Documents/618ti.pdf.

[45] Steven McFadyen, *Typical Three Phase Motor Currents*, 2012. [Online]. Available: https://myelectrical.com/notes/entryid/156/useful-motor-technical-information.

[46] H. Z. Kister, *Distillation Design*, 1st. New York: McGraw-Hill Education, 1992.

[47] R.K. Sinnott, 'Chapter 11: Separation Columns (Distillation, Absorption, And Extraction),' in *Chemical Engineering Design: Principles, Practice and Economics of Plant and Process Design*, Elsevier Inc., 2008. [Online]. Available: https://www.globalspec.com/reference/22824/203279/chapter-11-separation-columns-distillation-absorption-and-extraction.

[48] R. F. Strigle, *Random Packings and Packed Towers : Design and Applications*. Gulf Publishing Company, 1987.

[49] *Pall Rings*. [Online]. Available: https://www.machengineering.com/plastic-pall-rings/.

[50] A. Pérez Sánchez, E. J. Pérez Sánchez and R. Segura Silva, 'Design of a packed-bed absorption column considering four packing types and applying MATLAB,' *Nexo Revista Científica*, Dec. 2016.

[51] Sulzer, *SULCOL*. [Online]. Available: https://www.sulzer.com/en/shared/products/sulcol-for-windows.

[52] Standards Association of Australia, *Pressure vessels*. The Association, 1997.

[53] *Chemical Engineering Plant Cost Index - Chemical Engineering*. [Online]. Available: https://www.chemengonline.com/pci-home.

[54] J. Geng and H. Sun, 'Optimization and analysis of a hydrogen liquefaction process: Energy, exergy, economic, and uncertainty quantification analysis,' *Energy*, 2023.

[55] University of Toronto Research Administration, 'Guideline on Full Cost Recovery in Research,' Tech. Rep., 2020. [Online]. Available: https://research.utoronto.ca/media/108/download.

[56] DACE Cost and Value - The Dutch Network and Knowledge Center for Cost Engineering and Value Management, *DACE Price Booklet*, 33rd ed. Johan Schot, 2018.

[57] M. Afman, 'Energy and electricity price scenarios,' Tech. Rep., 2020. [Online]. Available: https://cedelft.eu/wp-content/uploads/sites/2/2021/04/CE_Delft_3H58_Energy_and_electricity_price_scenarios_DEF.pdf.

[58] AACE International, 'Cost Estimate Classification System,' Tech. Rep., 2020. [Online]. Available: https://aacei-pittsburgh.org/wp-content/uploads/2021/11/cost-estimating-classification-system.pdf.

[59] IRENA, 'ELECTRICITY STORAGE AND RENEWABLES: COSTS AND MARKETS TO 2030,' Tech. Rep., 2017. [Online]. Available: https://www.irena.org/publications/2017/oct/electricity-storage-and-renewables-costs-and-markets.

[60] F. Díaz-González, A. Sumper, O. Gomis-Bellmunt and R. Villafáfila-Robles, 'A review of energy storage technologies for wind power applications,' *Renewable and Sustainable Energy Reviews*, 2012.

[61] IRENA, 'Renewables and Electricity Storage: A technology roadmap for REmap 2030,' Tech. Rep., 2015. [Online]. Available: https://www.irena.org/-/media/Files/IRENA/Agency/Publication/2015/IRENA_REmap_Electricity_Storage_2015.pdf.

[62] B. Scrosati and J. Garche, 'Lithium batteries: Status, prospects and future,' *Journal of Power Sources*, 2010.

[63] H. Chen, T. N. Cong, W. Yang, C. Tan, Y. Li and Y. Ding, 'Progress in electrical energy storage system: A critical review,' *Progress in Natural Science*, 2009.

[64] M. R. Khan, M. J. Swierczynski and S. K. Kær, 'Towards an ultimate battery thermal management system: A review,' *Batteries*, Mar. 2017.

[65] J. R. Dahn, E. W. Fuller, M. Obrovac and U. von Sacken, 'Thermal stability of LixCoO2, LixNiO2 and λ-MnO2 and consequences for the safety of Li-ion cells,' *Solid State Ionics*, 1994.

[66] G. E. Blomgren, 'The Development and Future of Lithium Ion Batteries,' *Journal of the Electrochemical Society*, 2016.

[67] N. Nitta, F. Wu, J. T. Lee and G. Yushin, 'Li-ion battery materials: present and future,' *Materials Today*, Jun. 2015.

[68] M. Müller, L. Viernstein, C. N. Truong *et al.*, 'Evaluation of grid-level adaptability for stationary battery energy storage system applications in Europe,' *Journal of Energy Storage*, Feb. 2017.

[69] International Electrotechnical Commission (IEC), 'Electrical Energy Storage,' White paper, Tech. Rep., 2011. [Online]. Available: https://www.iec.ch/basecamp/electrical-energy-storage.

[70] D. Linden and T. B. Reddy, *Handbook of Batteries*, 3rd ed. McGraw-Hill, 2002. [Online]. Available: http://www.inexess.com/files/ecar/Akkus/Handbook%20Of%20Batteries%203rd%20Edition.pdf.

[71] B. Li and J. Liu, 'Progress and directions in low-cost redox-flow batteries for large-scale energy storage,' *National Science Review*, Jan. 2017.

[72] A. Z. Weber, M. M. Mench, J. P. Meyers, Ross. Philip N., J. T. Gostick and Q. Liu, 'Redox flow batteries: a review,' *Journal of Appled Electrochemistry*, 2011.

[73] M. Skyllas-Kazacos, M. H. Chakrabarti, S. A. Hajimolana, F. S. Mjalli and M. Saleem, 'Progress in Flow Battery Research and Development,' *Journal of The Electrochemical Society*, 2011.

[74] A. Luvishis, L. Luvishis and I. Luvishis, *Hybrid Rail Vehicles*. 2010.

[75] X. Luo, J. Wang, M. Dooner and J. Clarke, 'Overview of current development in electrical energy storage technologies and the application potential in power system operation,' *Applied Energy*, Jan. 2015.

[76] D. H. Doughty, P. C. Butler, A. A. Akhil, N. H. Clark and J. D. Boyes, 'Batteries for Large-Scale Stationary Electrical Energy Storage,' *The Electrochmical Society Interface*, 2010.

[77] R. Benato, N. Cosciani, G. Crugnola *et al.*, 'Sodium nickel chloride battery technology for large-scale stationary storage in the high voltage network,' *Journal of Power Sources*, Oct. 2015.

[78] R. S. James Burgess, *Rotterdam aims to supply 4.6 million mt/year of hydrogen by 2030*, 2023. [Online]. Available: https://www.spglobal.com/commodityinsights/en/market-insights/latest-news/electric-power/051022-rotterdam-aims-to-supply-46-million-mtyear-of-hydrogen-by-2030.

[79] COHO an ERM Group company, *The Pros and Cons of a Power Purchase Agreement (PPA) & How They Work*. [Online]. Available: https://www.cohoclimate.com/blog/ppas-explained/.

[80] D. U. Sauer, G. Fuchs and M. Leuthold, 'Technology Overview on Electricity Storage-Overview on the potential and on the deployment perspectives of electricity storage technologies,' Tech. Rep., 2012. DOI: 10.13140/RG.2.1.5191.5925.

A

Appendix A

A.1. Wind data

The wind data used for the leakage estimations as well as the modeling of battery systems is based on the HKN offshore wind farm. The attached wind power data is based on the year 2019 and scaled to an average capacity of 100 MW.

A.2. Leakage calculations

More details of leakage estimations, described in chapter 3, are provided in the tables A.1, A.2, A.3, A.4, A.5, and A.6.

Table A.1: Emission calculations

Venting due to unavailability of power		
Venting during single shutdown (due to loss of power-only electrolyzer unit)	10*(Volume of catholyte header tank + Volume of H_2 gas cooler + Volume of H_2 gas filter + Volume of piping involved) in 10 MW electrolysis unit	
	221	m_3
Mass of hydrogen vented	15.3	kg
Hydrogen production 100 MW at 100%	1792	kg/hr
Hydrogen production at 15% capacity	268.8	kg/hr
Venting during single startup (due to loss of power-only electrolyzer unit) (Assumed to take 2 hrs to reach desired spec)	2hrs*(Continuous production in 100 MW unit during 2 hrs of venting)	
	537.5	kg
Total number of shutdowns in one year (due to unavailability of power)	156	
Net venting due to shutdowns	Number of shutdowns* Venting during single shutdown	
	2378.8	kg
Total number of startups in one year (due to unavailability of power)	156	
Net venting due to startups	Number of startups * Venting during single startup	
	83850	kg
Venting due to unavailability of power	86228.8	kg
Number of hours in one year when the unit is shutdown due to unavailability of power	1254.5	hrs

A

Table A.2: Emission calculations

Venting due to planned maintenance & emergency shutdowns		
Number of hours lost in planned maintenance or emergency shutdown combined	438	hrs
PDU and compressor units are shutdown	Once every 2 years	
Only electrolysis units are in planned maintenance while PDU and compressor are pressurized	Once every 8 years	
Planned maintenance	375.1	kg
Emergency shutdown	All the units are vented (once every year)	
Volume of each compressor and PDU unit combined	25	m_3
Mass of hydrogen vented out of each compressor and PDU unit combined	98.7	kg
Shutting down	212.7	kg
Hydrogen unit production at 3% capacity	53.8	kg/hr
Starting up (4 hrs of venting at 3% turndown capacity)	5160	kg
Emergency shutdowns	5372.7	kg
Venting due to hydrogen crossover		
From heat and bass balance of the units, 0.41 mol% hydrogen is estimated to be vented with the oxygen produced in the electrolysis unit		
Rate of hydrogen crossover	3.6	kg/hr
Number of hours in one year when the unit is operational (O2 will be vented at all times)	7067.5	hrs
Hydrogen crossover	25301.7	kg
Operational purging		
Hydrogen vented through one measurement analyzer	0.037	kg/hr
Total number of analyzers	8	
Venting through analyzers	0.3	kg/hr
Venting through analyzers in one year	2119.2	kg
Venting from demineralized water purification unit	6.7* 10^-5	kg/hr
Number of hours the unit is operational	7067.5	
Venting from demineralized water purification unit in one year	0.47	kg
Operational purging	2119.6	kg

Table A.3: Emission calculations

Leakages in flanges and valves		
Emission rate of CH_4 from all components of a given type in the stream ($E(CH_4)$)	Average emission factor for the component type A* Average wt fraction of CH_4* Number of components of the given type in the stream * Number of hrs unit is online	
$E(H_2)$	$3*E(CH_4)*$Mol wt of H_2/Mol wt of CH_4	
Leakages in flanges, seals and valves	4558.4	kg
H_2 production in one year	12662.6	tons
Vented H_2 (except fugitive leakages)	119.4	tons
Fugitive leaks from flanges, valves and seals	18.2	tons
Total	137.6	tons
Net H_2 emissions (taking into account 10% ignition)	123.8	tons
Net H_2 production over the year (excluding vented H_2)	12525	tons
	12662.6	
Amount emitted out of total produced	0.98%	
Europe is expected to have 574 GW H_2 from electrolysis by 2050		
For simplicity, we assume 574000 MW can be done by taking 5740 trains of 100 MW capacity each.		
Total emissions for 5740 trains of 100 MW capacity each	789852.1	tons
Net H_2 emissions (taking into account 10% ignition)	710866.9	tons

Table A.4: Number of components in the electrolysis unit

	Flanges	Valves	Control valves	PSVs	Compressor seals	H_2 (wt%)
Catholyte Header tank system	11	1	-	-	-	66.20%
Hydrogen treatment (H_2 filter, cooler)	21	8	4	-	-	66.20%
No. of modules=10	320	90	40	0	-	66.20%
H_2 Compression (2 compressor units with common inlet and outlet headers)						
Inlet Header	29	9	2	-	-	66.20%
1st stage	43	4	3	2	1	66.20%
For 2 units	86	8	6	4	2	66.20%
2nd stage	39	4	-	1	1	79.90%
For 2 units	78	8	-	2	2	79.90%
3rd stage	38	4	-	1	1	89.30%
For 2 units	76	8	-	2	2	89.30%
4th stage	32	2	-	1	1	94.50%
For 2 units	64	4	-	2	2	94.50%
5th stage	34	4	-	1	1	100.00%
For 2 units	68	8	-	2	2	100.00%
Outlet Header	6	5	4	-	-	100.00%
LP H_2 product system	36	39	2	-	-	100.00%
H_2 Compression unit battery limit	16	25	1	-	-	100.00%
PDU unit	48	14	10	2	-	97.25%
2 PDU units	96	28	20	4	-	97.25%
H_2 Metering & Battery Limit	34	63	12	-	-	100.00%

Table A.5: Emission factors

From energy API (Compendium of greenhouse gas emissions methodologies for the oil and natural gas industry, August 2009 [30])			
	Flanges	Valves	Others
Emission Factor (tonne/hr/component)	$4.38*10^{-7}$	$3.86*10^{-6}$	$4.86*10^{-6}$
From actual vendor experience			
	Compression leakage - normal operation	Compression leakage- pressurized standstill	
Leakage rate (kg/hr)	0.89	1.52	

Table A.6: Calculation results of fugitive leakages from flanges, valves and seals in the unit

	Flanges	Valves	Control valves	PSVs
Total electrolysis unit (No. of modules = 10)	0.66	1.63	0.91	-
H_2 Compression (2 compressor units with common inlet and outlet headers)				
Inlet header (tons)	0.06	0.16	0.05	-
1st stage (tons)	0.18	0.14	0.14	0.09
2nd stage (tons)	0.19	0.17	-	0.05
3rd stage (tons)	0.21	0.19	-	0.06
4th stage (tons)	0.19	0.10	-	0.06
5th stage (tons)	0.21	0.22	-	0.07
Outlet header (tons)	0.02	0.14	0.14	-
LP H_2 product system (tons)	0.11	1.06	0.07	-
H_2 Compression unit battery limit (tons)	0.05	0.68	0.03	-
2 PDU units (tons)	0.29	0.74	0.67	0.13
H_2 Metering & Battery Limit (tons)	0.11	1.72	0.41	-
Total(tons)	2.27	6.97	2.41	0.47

B

Appendix B

B.1. De-hydro model validation results

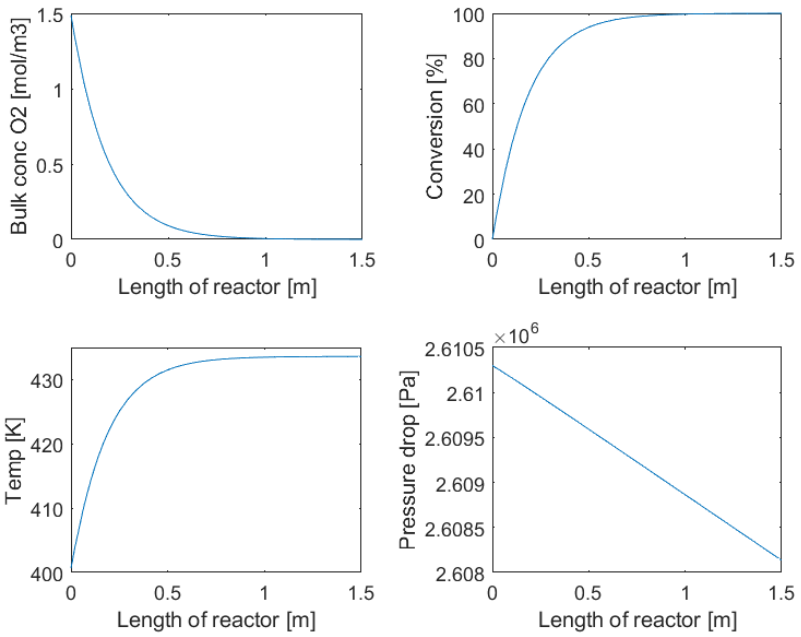

Figure B.1: Results of de-hydro model validation

B

B.2. Stream summaries of proposed designs

Table B.1: Stream summary of Design 1

Stream name	Vapor fraction	Temperature (°C)	Pressure (kPa)	Molar flow (kgmole/h)	Mass flow (kg/h)	Mole fraction (H_2)	Mole fraction (H_2O)	Mole fraction (O_2)
Saturated gas stream	1.00	50.00	130.00	534.90	16345.85	0.00	0.10	0.90
1-1	1.00	134.83	280.80	534.90	16345.85	0.00	0.10	0.90
1-2	1.00	134.83	280.80	534.90	16345.85	0.00	0.10	0.90
1-3	0.00	134.83	280.80	0.00	0.00	0.00	1.00	0.00
1-4	1.00	72.56	279.00	554.15	16692.74	0.00	0.13	0.87
1-5	0.00	73.79	279.00	223.84	4032.55	0.00	1.00	0.00
Bleed stream	0.00	73.79	279.00	22.38	403.26	0.00	1.00	0.00
1-6	0.00	72.56	279.00	0.00	0.00	0.00	1.00	0.00
1-7	0.00	73.79	279.00	201.46	3629.30	0.00	1.00	0.00
Recycle	0.00	73.82	600.00	201.46	3629.30	0.00	1.00	0.00
Make-up water	0.00	10.00	500.00	41.63	750.00	0.00	1.00	0.00
1-8	0.00	62.95	500.00	243.09	4379.30	0.00	1.00	0.00
1-9	0.00	62.96	500.00	243.10	4379.45	0.00	1.00	0.00
To-dehydro reactor	1.00	72.56	279.00	554.15	16692.74	0.00	0.13	0.87

Table B.2: Stream summary of Design 2

Stream name	Vapor fraction	Temperature (°C)	Pressure (kPa)	Molar flow (kgmole/h)	Mass flow (kg/h)	Mole fraction (H_2)	Mole fraction (H_2O)	Mole fraction (O_2)
Saturated gas stream -2	1.00	50.00	130.00	534.90	16345.85	0.00	0.10	0.90
2-1	1.00	134.83	280.80	534.90	16345.85	0.00	0.10	0.90
2-2	1.00	134.83	280.80	534.90	16345.85	0.00	0.10	0.90
2-3	0.00	134.83	280.80	0.00	0.00	0.00	1.00	0.00
2-4	1.00	72.56	279.00	554.15	16692.74	0.00	0.13	0.87
2-5	0.00	73.79	279.00	223.84	4032.55	0.00	1.00	0.00
Bleed stream 2-1	0.00	73.79	279.00	22.38	403.26	0.00	1.00	0.00
2-6	0.00	72.56	279.00	0.00	0.00	0.00	1.00	0.00
2-7	0.00	73.79	279.00	201.46	3629.30	0.00	1.00	0.00
Recycle 2-1	0.00	73.82	600.00	201.46	3629.30	0.00	1.00	0.00
Make-up water 2-1	0.00	10.00	500.00	41.63	750.00	0.00	1.00	0.00
2-8	0.00	62.95	500.00	243.09	4379.30	0.00	1.00	0.00
2-9	0.00	62.96	500.00	243.10	4379.45	0.00	1.00	0.00
2-10	1.00	72.56	279.00	554.15	16692.74	0.00	0.13	0.87
To-dehydro reactor 2-1	1.00	130.00	274.00	554.15	16692.74	0.00	0.13	0.87

Table B.3: Stream summary of Design 3

Stream name	Vapor fraction	Temperature (°C)	Pressure (kPa)	Molar flow (kgmole/h)	Mass flow (kg/h)	Mole fraction (H_2)	Mole fraction (H_2O)	Mole fraction (O_2)
Saturated gas stream -3	1.00	50.00	130.00	534.90	16345.85	0.00	0.10	0.90
3-1	1.00	134.83	280.80	534.90	16345.85	0.00	0.10	0.90
3-2	0.94	45.00	275.80	534.90	16345.85	0.00	0.10	0.90
3-3	1.00	45.00	275.80	501.69	15747.56	0.00	0.04	0.96
3-4	0.00	45.00	275.80	33.21	598.29	0.00	1.00	0.00
3-5	1.00	129.53	595.73	501.69	15747.56	0.00	0.04	0.96
3-6	0.98	45.00	590.73	501.69	15747.56	0.00	0.04	0.96
3-7	0.00	45.00	590.73	9.36	168.61	0.00	1.00	0.00
3-8	1.00	45.00	590.73	492.33	15578.96	0.00	0.02	0.98
To-dehydro reactor 3	1.00	129.93	1275.97	492.33	15578.96	0.00	0.02	0.98

B.3. Economic Analysis

The section 4.2.8.3 discusses the cost estimation results of the three proposed designs. Design 2 was discovered to be the most cost-effective, and a breakdown of capital costs is provided in the main section. FigureB.2 also shows the breakdown

of capital costs for designs 1 and 3. Design 3 is the most capital-intensive as it has 3 compressors.

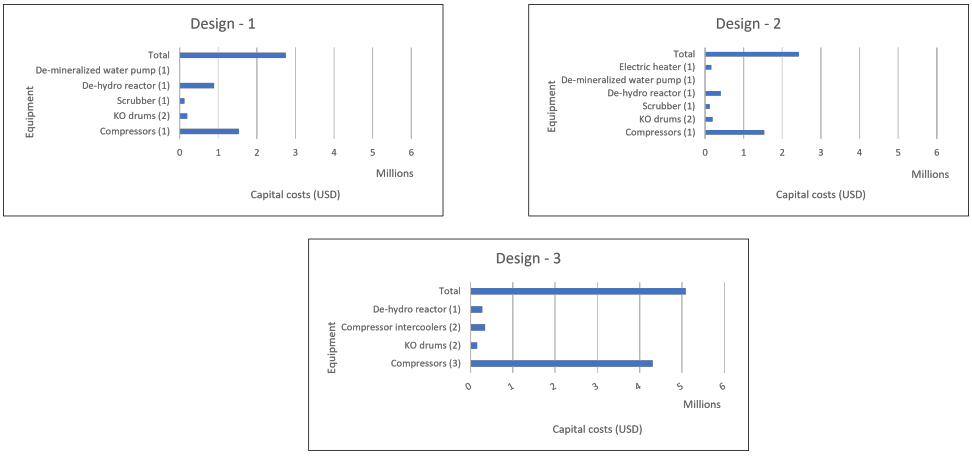

Figure B.2: Capital costs breakdown

C

Appendix C

C.1. Different BES technologies

Section 4.3.1 discusses the various battery energy technologies. Fundamental workings of these different battery cells are illustrated in the figures C.1, C.2, C.3 and C.4.

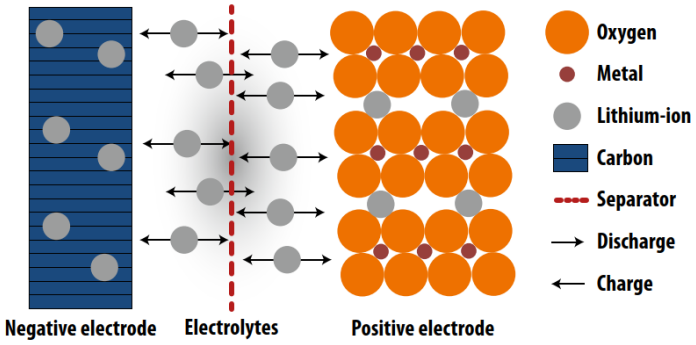

Figure C.1: Li-ion battery technology [80]

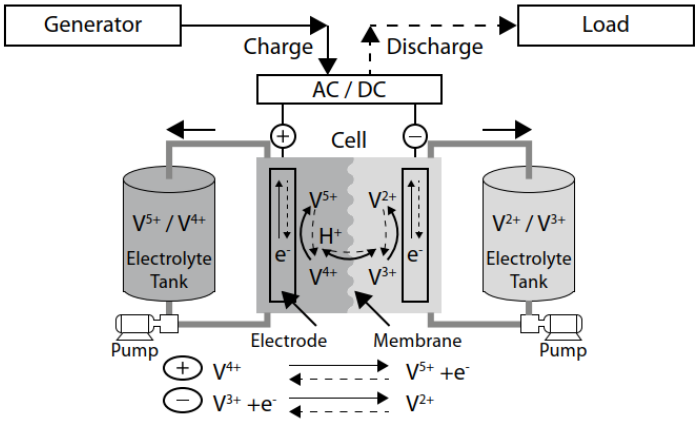

Figure C.2: Vanadium redox flow battery technology [70]

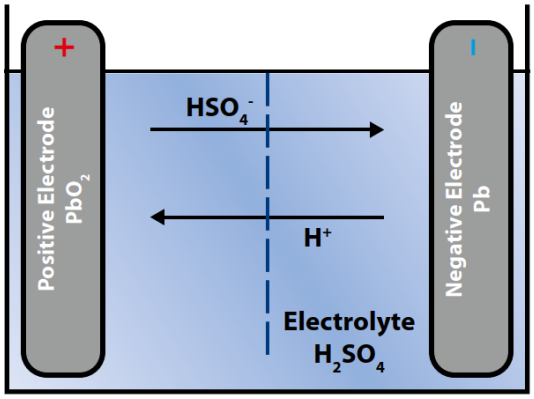

Figure C.3: Sealed lead acid battery technology [80]

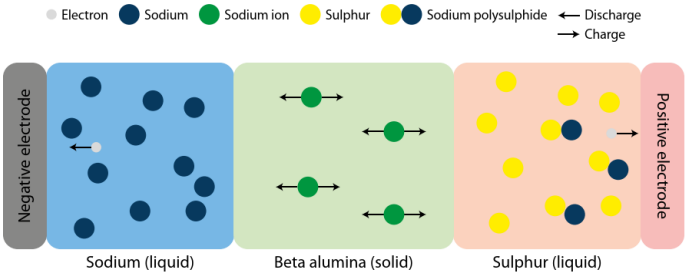

Figure C.4: Sodium sulfur battery technology [80]

C.2. Sensitivity analysis on VRFB battery systems

To do a sensitivity study, the following parameters are changed by +/-50% from their base value.
1) Cost of N_2 required for purging
2) Cost of CO_2 equivalents of hydrogen emissions
3) Price of green H_2
4) Capital cost of battery system
The findings of the sensitivity analysis are discussed in the section 4.3.4. Figures C.5, C.6, C.7 and C.8 show the cost trends when each of the variables mentioned above is changed. As stated in the section 4.3.4, the figures show that total costs are least sensitive to changes in nitrogen costs and most sensitive to changes in BES costs.

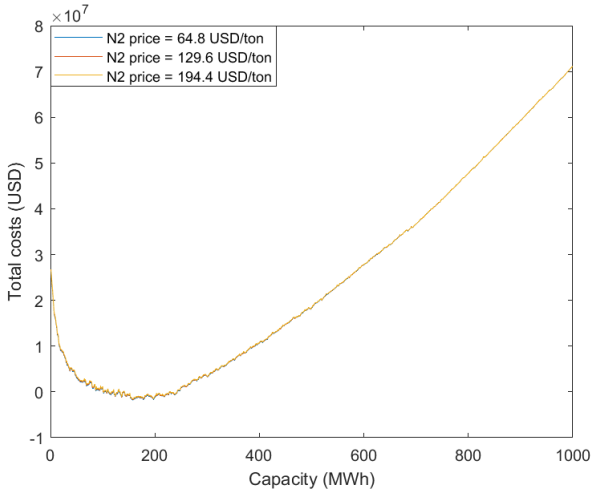

Figure C.5: Sensitivity by varying purging cost of nitrogen

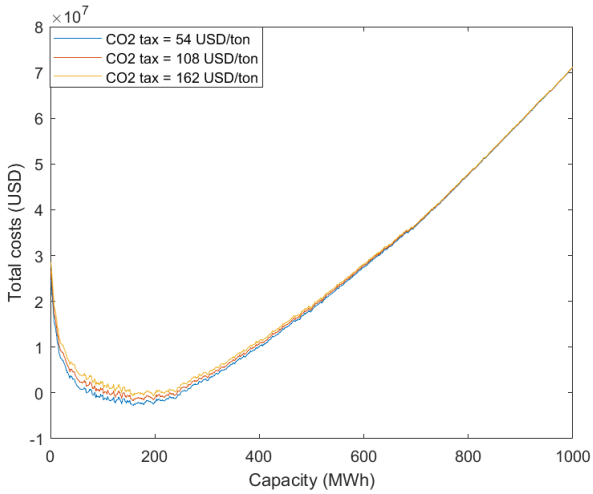

Figure C.6: Sensitivity by varying tax on hydrogen/CO2 equivalents

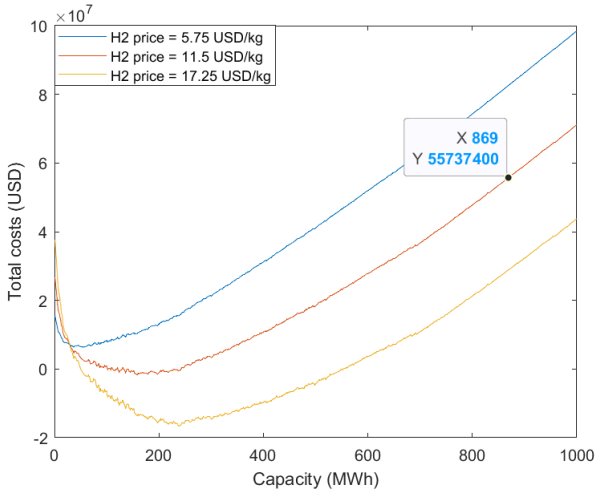

Figure C.7: Sensitivity by varying price of green hydrogen

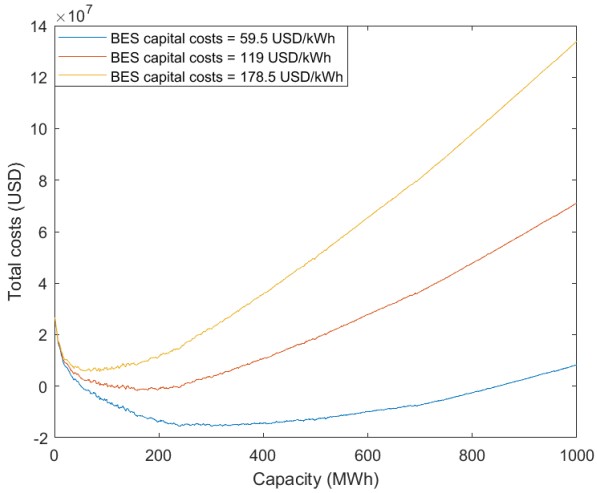

Figure C.8: Sensitivity by varying capital costs of BES

C.3. Comparison of different BES technologies

Different battery technologies are compared and the results are discussed in the section4.16. Vanadium flow battery systems offer the highest optimal capacity and maximum incentives after installation. Figures C.9, C.10, C.11, C.12 and C.13 show the cost versus capacity trends of other battery technologies. These figures also show that, after VRFB, Li-ion NCA battery systems perform the best in terms of optimal capacity and overall costs.

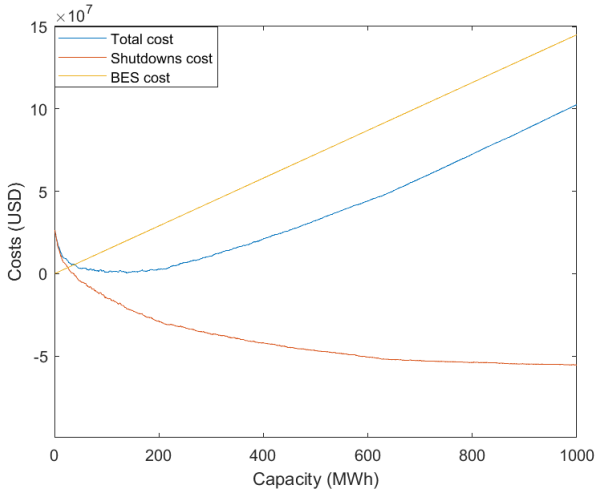

Figure C.9: Cost vs capacity of NCA Li-ion battery systems

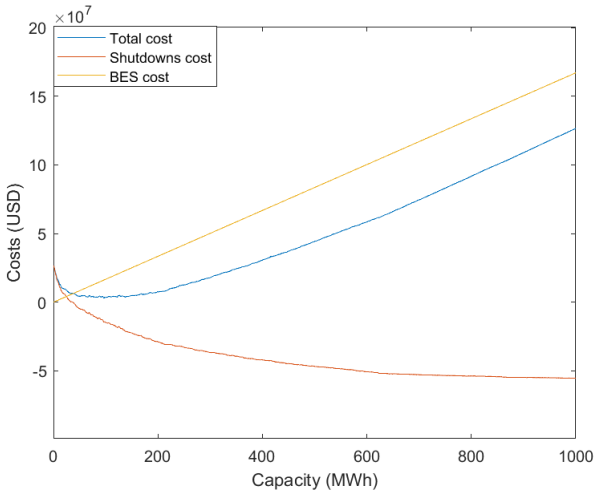

Figure C.10: Cost vs capacity of NMC Li-ion battery systems

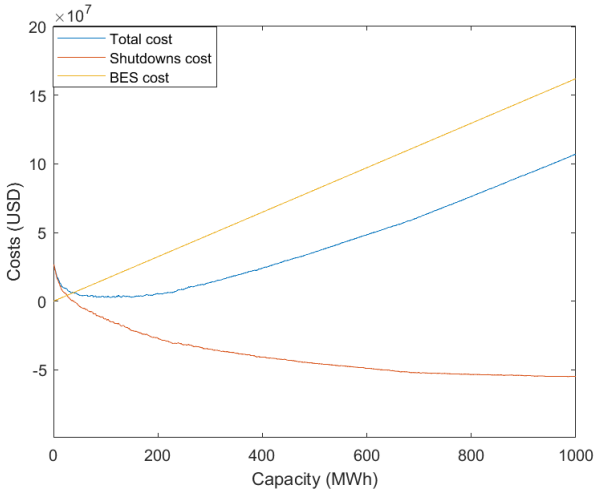

Figure C.11: Cost vs capacity of sodium sulfur battery systems

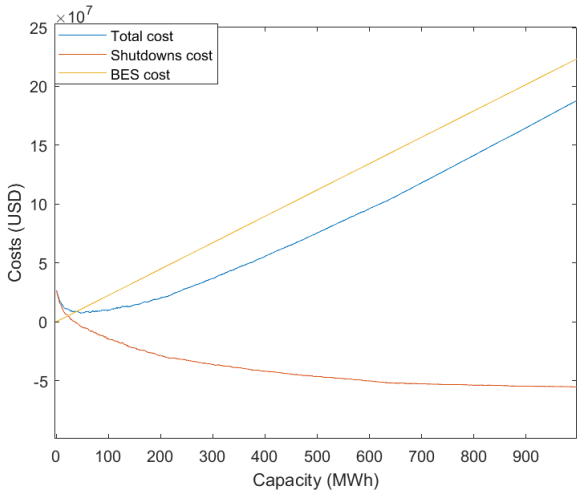

Figure C.12: Cost vs capacity of LFP Li-ion battery systems

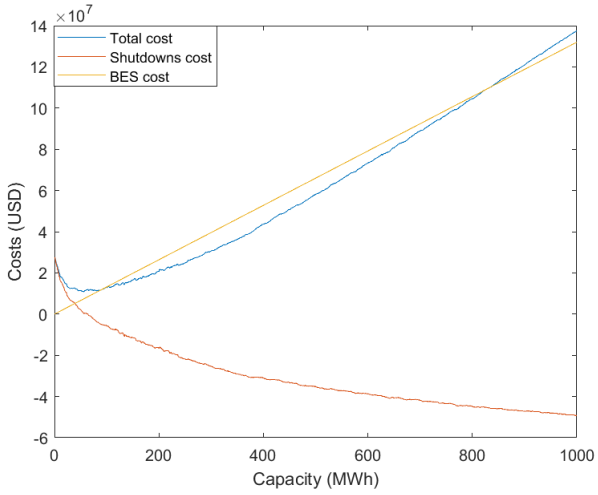

Figure C.13: Cost vs capacity of sealed lead-acid battery systems